

## **Decoding the hysteretic behavior of hydraulic variables in lowland rivers with multivariate monitoring approaches**

M. Muste<sup>1</sup>, K. Kim<sup>1,2</sup>, D. Kim<sup>2</sup>, G. Fleit<sup>3</sup>

<sup>1</sup> IIHR-Hydroscience & Engineering, University of Iowa, Iowa City, Iowa, USA.

<sup>2</sup> Civil & Environmental Engineering, Dankook University, Yongin, Gyeonggi, South Korea.

<sup>3</sup> Hydraulic & Water Resources Engineering, Budapest University of Technology & Economics, Budapest, Hungary

This paper demonstrates that the multivariate monitoring methods are capable to underpin the systematic investigation of the hysteretic behavior occurring during gradually-varied flows. For this purpose, we present simultaneous measurements of stage, index velocity, and free-surface slope acquired continuously with high-frequency sampling instruments deployed at several river gauging sites exposed to a range of storm magnitudes. The experimental evidence reveals intrinsic features of unsteady open-channel flow mechanics that are hinted by pertinent governing equations but rarely substantiated with in-situ measurements. The illustrations are intentionally made for fluvial waves propagating at sites located in lowland areas where the relationships among flow variables are most likely displaying hysteretic loops and phasing in the hydraulic variable progression. The set of presented measurements highlights that: a) the hysteretic behavior is apparent in both time-independent and time-dependent graphical representations of any two of the hydraulic variables; b) the severity of the hysteresis is commensurate with the geomorphic, hydraulic, and hydrological characteristics of the measurement site; and c) there is a pressing need for changing the flow paradigms currently used in tracking flow variables during gradually-varied flows. Also discussed are research needs associated with flow hysteresis for advancing the understanding of the mechanisms underlying the movement and storage of water in the lowland river environments as well as for increasing the accuracy of streamflow monitoring, modeling, and forecasting.

Keywords: hysteresis, lowland rivers, streamflow monitoring, fluvial waves, unsteady channel flows

---

This manuscript is an EarthArXiv preprint and has been submitted for possible publication in a peer-reviewed journal. Please note that this has not been peer-reviewed before and is currently undergoing peer review for the first time. Subsequent versions of this manuscript may have slightly different content.

---

## 1. Introduction

The highly dynamic conditions associated with repeated wet-dry cycles in lowland and plain rivers lead to gradual movement and/or storage of water in the channel network that inherently produce hysteresis (e.g., Henderson, 1966, Fenton, 2001). Hysteresis is a property of a physical system to produce different process outcomes depending on the trajectory of the changes in the independent variables (Prowse, 1984). This property results in non-unique relationships and time lags between any two independent variables of the process. Initially related to the effect of magnetization (Ewing, 1882), the hysteretic behavior has been studied in multiple contexts, from physics, chemistry, engineering, and biology, to economics. In the present paper, the focus is on the hysteresis among hydraulic variables during cyclical unsteady flows (a.k.a. fluvial waves) whereby “loops” and “lags” between flow variables are apparent on the rising and falling limbs of the hydrographs. Given that hysteretic behavior in open-channel flow is most often related to loops in the simple stage-discharge relationships (a.k.a. ratings), the hysteresis is labeled as “loop rating” (Kennedy, 1984) or “loop-rating curve” (Henderson, 1966).

Hysteresis has been also identified in the relation between streamflow determined with the simple stage-discharge ratings and a large number of other hydrological variables such as precipitation, groundwater level, soil moisture, hillslope flows, transported materials in open channel (e.g., Kumar, 2011; Zuecco et al., 2015). In contrast with hydrological processes, the hysteretic loops and phasing occurring among hydraulic variables in gradually-varied open-channel flows are rarely captured in situ as the acquisition of direct measurements is rarely done over the whole duration of the fluvial wave propagation while the continuous measurements for streamflow monitoring track only one or two hydraulic variables that does not fully cover hysteresis manifestation. In the absence of direct measurements and given that the nonlinear governing equations describing hysteresis in natural streams are difficult to solve for practical problems, there is a general consensus that the nonuniform and unsteady flows in river networks continue to remain understudied. Relatedly, there is a status quo in fully understanding and interpreting the impact of these flows on a variety of riverine transport and environment processes.

The present paper deals with in-stream hysteresis occurring during nonuniform and unsteady flows (a.k.a. gradually-varied flows or long fluvial waves) confined within the stream bank elevation. These flows are labeled as moderate flow domain in Figure 1a. Above the “Action flood” line shown in this figure, the stream flows over into the floodplain complicating the hysteretic behavior interpretation. Given their persistence, fluvial waves have a greater influence on the river environment compared to the periods of steady flows that usually take less than 50% of the annual flows as shown Figure 1b for a Midwestern stream. Understanding these influences are critical for managing waterways and flood mitigation efforts as well as for studies on river morphology and ecology (Tabarestani & Zarrati, 2015). While hysteresis is inherent during the propagation of long fluvial waves, its strength depends on the site and flow characteristics. Lowland rivers exposed to high and fast-developing fluvial waves are certainly situations where hysteresis is of concern (Thebault et al 2023). Fluvial waves are currently more frequent and severe due to climatic changes, often leading to devastating floods (Mallakpour & Villarini, 2015).

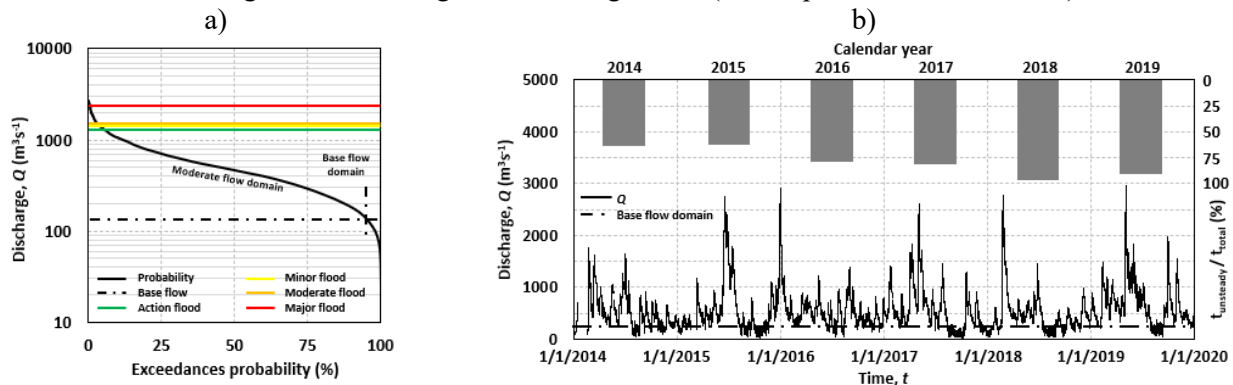


Figure 1. Hydrological conditions for the USGS #005558300 gaging site on Illinois River: a) flow exceedance probability. Flood warning lines from: <https://water.weather.gov/ahps/>; and b) illustration of unsteady flow pervasiveness

The investigation of the nonuniform and unsteady flows has been central for theoretical, laboratory, and in-situ explorations since its substantiation more than 150 years ago (Hager et al., 2019). The knowledge concerning these flows is summarized in numerous textbooks (e.g., Chow, 1959; Henderson, 1966; Ponce, 1989) and published research covering the topic from fluid dynamics, applied hydraulics or hydrology perspectives (e.g., Moots, 1938; Nezu & Nakagawa, 1995; Dottori et al., 2009; Mrokowska et al., 2015; Fenton, 2019; Dykstra & Dzwonkowski, 2020; Marcus et al., 2023). The current mathematical framework for the analysis of this type of flows is provided by the Saint-Venant equations (Saint-Venant, 1871). Obtaining exact solutions for these partial differential equations is considered one of the most difficult fluid mechanics problems generating an interest materialized in doubling the amount of references every 15 years (Yevdjovich, 1964). Despite the exponential increase in efforts, acceptable solutions are only available for a limited number of practical problems. Moreover, the outcomes of theoretical studies are rarely validated with experiments as the data from laboratory studies are affected by multiple scale-induced distortions and the much-needed data from natural streams are rarely available (Muste et al., 2020) or uncertain (di Baldassare & Montanari, 2009).

The most appropriate approach to observe the hysteresis process in its natural evolution is the acquisition of direct in-situ measurements for all the hydraulic variables. The planning and execution of direct measurements in the field are however demanding as they require identification of sites with measurable hysteresis, proper preparation to start the measurements at the time of the steady flow disturbance, and the design and execution of an adequate measurements strategy to capture the wave characteristics with high sampling rates over the whole duration of the wave propagation that can extend to days or even months. It is obvious that these demanding prerequisites are difficult, or sometime, impossible to render through typical investigations. A more effective approach to observe the hysteresis behavior is to extract its signature from measurements acquired in unsteady flows at existing streamflow gaging stations operated by specialized agencies. At the monitoring stations direct measurements of hydraulic variables such as stage, index velocity, or free-surface slope are continuously taken to be used with rating curves. These ratings are previously developed for each type of station (i.e., stage-discharge, index-velocity) using graphical methods applied to direct measurements relating one of the flow variables with streamflow measured directly with other methods and instruments (Rantz, 1982; Levesque and Oberg, 2012; Muste et al., 2019). The directly measured flow variables are inherently affected by hysteresis. However, the discharge provided by existing ratings totally miss or only partially reflect hysteresis as they are constructed under the assumption of piece-wise steady flow that obviously is not valid during unsteady flows.

The most problematic rating for discharge estimation in unsteady and nonuniform flows is the widely used stage-discharge rating curves (labeled herein HQRC). The agencies are aware of the HQRC limitations (Holmes, 2016) and, for selected sites, corrections are applied to the data after they are acquired (Kennedy, 1984; Schmidt & Garcia, 2013). However, due to high costs associated with the corrections, the vast majority of the stage-discharge ratings remain uncorrected. More helpful for discharge estimation in these flows is the index-velocity method (IVRC) that measures continuously an index velocity (a dynamic flow parameter sampled in a point, along a line or over a surface) in addition to stage (Levesque & Oberg, 2012; Hoitink, 2018). Another discharge estimation approach that performs well in unsteady and nonuniform flows is the continuous slope-area method (CSA) where simultaneous stage measurements are taken at two locations to provide free-surface slope in addition to the stage (Muste et al., 2019). Because IVRC and CSA methods entail continuous measurements of two hydraulic variables, we label them as multivariate monitoring methods to distinguish from the bivariate relationships at HQRC stations. The conventional IVRC and CSA monitoring approaches were revitalized by the assimilation of contemporary instruments, mostly based on acoustic principles. Details on the capabilities of exiting monitoring methods document hysteresis flows are discussed in Muste et al. (2020) and Muste et al. (2022a).

Given the limited reliance on the unsteady and nonuniform flow data resulting from analytical, numerical simulations, laboratory-scaled models, and conventional streamflow monitoring there is an acute need for tackling the shallow-water equations for the mass, momentum, and energy conservation with new data-driven approaches that make use of in-situ data collected continuously with appropriate measurement approaches. It is deemed that such an investigative path can elucidate the intricate features of hysteresis and its sensitivity to hydraulic/hydrological parameters (e.g., wave intensity and attenuation, bed roughness and slope). A promising development line in this regard is to build on the proof-tested IVRC and CSA methods that are superior to the HQRC performance in unsteady, nonuniform flows. While none of the multivariate monitoring methods are fully characterizing hysteresis, they offer a proper basis for the proposed development. The research associated with this new data-driven approach should necessarily include systematic investigations on the hysteretic effects on the performance of the rating-based monitoring methods to estimate unsteady and nonuniform flows. This paper is a first step along the this development.

The measurements across sites and events presented in the paper seek for demonstrating that the IVRC and CSA methods capture partially symptoms and behavior of hydraulic variables that reflect most of our current knowledge on hysteresis as derived from other sources. A secondary role of the presented experimental evidence is to explore new, physically-based, in-situ discharge monitoring approaches that are capable to quantify streamflow in steady and unsteady conditions. When referring to discharge estimation, the present discussion attempts to depart from the premises of the conventional streamflow monitoring methods of the past whereby semi-empirical and statistical approaches are used to develop relationships among variables, i.e., ratings. Instead, we prompt to the possibility to directly estimate streamflow using continuously measured variables sampled appropriately over space and time in conjunction with the hysteresis theoretical framework. This data-driven approach also contrasts with the physically-based simulation models where analytical formulations are embedded in numerical schemes to obtain discharges along the stream under imposed initial and boundary conditions. Obtaining discharges using explicit relationships among independent variables is labeled as the “inverse” solution to distinguish it from the “forward” solution used by numerical simulations (Wunsch, 2019). The inverse solution for discharge estimation has limited reliance on ratings excepting those involving the characterization of the measurement site, based typically of a one-time geodetical survey.

The paper is organized as follows. First, we present features derived from the theoretical knowledge on the hysteresis process and its progression in time and space. Next, we mirror the conceptual understanding with data acquired in-situ at various sites and across several events as reflected by measurements with multivariate monitoring approaches. Finally, we discuss the lines of research that can transition the current streamflow monitoring practice to more accurate approaches for assessing both steady and unsteady flows.

## **2. Hydraulic considerations and practical inferences on hysteresis behavior**

### ***Analytical considerations***

The type of hysteresis discussed herein is strictly related to aspects of translatory wave movement through gentle slope (lowland) channels whereby the entire body of water propagates as nonuniform and unsteady flood wave. The discussion assumes that unsteadiness-induced hysteresis acts in isolation from other potential causes (e.g., effects of instream vegetation, bedform-induced roughness development, and baseflow-stream interactions). The presented analysis adopts the hydraulic theoretical framework for long fluvial wave movement rather than the hydrological view of flood routing whereby multiple assumptions and approximations are typically used to solve the wave propagation.

The theoretical framework for unsteady open-channel flows is grounded on the long-standing formulation of the Saint-Venant equations derived from principles of mass and momentum conservation applied to shallow-water flows (Chow, 1959). These 1-D equations are valid for variable discharge and water storage (backwater) situations under the following assumptions: incompressible fluid, one-dimensional flow, hydrostatic pressure distribution, and negligible vertical acceleration. It should be mentioned that these conditions are essentially met if the best practice for site selection (Rantz et al., 1982) are strictly enforced, i.e., quasi-prismatic, straight channels without lateral inflows or outflows.

The Saint-Venant equations can be expressed in a variety of forms. For the present context, where we substantiate practical means to capture discharge with direct in-situ measurements, we use a form of these equations that are suitable for measurements of flow variables using one or two locations on a stream. Such a useful relationship is the arrangement provided by Knight (2006) that relates the discharge in unsteady flow,  $Q$ , with the steady discharge,  $Q_0$ , as defined by Equation (1):

$$Q = Q_0 \sqrt{1 - \frac{1}{S_0} \frac{\partial h}{\partial x} - \frac{V}{gS_0} \frac{\partial V}{\partial x} - \frac{1}{gS_0} \frac{\partial V}{\partial t}} \quad (1)$$

kinematic wave  $\rightarrow\rightarrow|$   
diffusive wave  $\rightarrow\rightarrow\rightarrow\rightarrow\rightarrow\rightarrow|$   
full dynamic wave  $\rightarrow\rightarrow\rightarrow\rightarrow\rightarrow\rightarrow\rightarrow\rightarrow|$   
with  $Q_0 = (1/n)AR^{2/3} \sqrt{S_0}$  (2)

Equation (2) is stated for metric units and contains the Manning's roughness coefficient,  $n$ , the channel cross-sectional area,  $A$ , the hydraulic radius,  $R$ , and the bed slope,  $S_0$ . The Manning's roughness coefficient is typically picked as a rough value from look-up tables (e.g., Arcement et al., 1989). The notations for the other variables are specified in Figure 2. Given that the flow depth,  $h$ , is derived from the stage,  $H$ , in hydrometric applications, their use herein is interchangeable (i.e.,  $(\partial h/\partial x) = (\partial H/\partial x)$  in the Figure 2). The first term in the equation is usually by far the largest term, therefore the bulk of the flood wave moves as a kinematic wave (Henderson, 1966). The third and fourth terms are usually of the same magnitude order. For steep rivers, the first term is dominant and the associated kinematic wave propagates only in the downstream direction. For flat slopes all terms may be significant and the associated dynamic wave propagates both in the downstream and upstream directions leading to wave subsidence (House et al., 2024).

Finding forward solutions with numerical models for Equation (1) is a complex and difficult task therefore recourse is made to simplifying approximations both for the underlying equation as well as for the initial and boundary conditions (Yevdjovich, 1964). However, it should be mentioned that even if the forward solution would be attainable, the results obtained with Equation (1) cannot be fully validated as there is rarely proper benchmark data tracking the flood wave propagation over its whole duration. Attempting the inverse solution for solving the unsteady flow governing equation is a promising path but it requires direct and continuous measurements of stage and bulk velocity at one or two locations in the stream. At this time, there are no formal monitoring methods that can deliver these measurements.

Given that a secondary goal of this paper is to screen relationships for discharge estimation from direct measurements taken at a single river section and using only stage measurements (as they are easier to get), we explore below manipulations for Equation (1) that use defensible assumptions, simplifications, or approximations. An elegant solution is analytically derived by Henderson (1966) for determining the discharge for mild waves (i.e., long and slow-rising fluvial waves). Using purely physical and analytical geometry considerations, Henderson offers a discharge formula (see equation 9-93) that can be used with measurements at one location. We do not present this version of the momentum equation as the associated assumptions restrict its use to only small Froude numbers and neglect the last two terms in Equation (1). Described below are two simplified formulations of Equation (1) that are neglecting only the local flow acceleration (the last term in the equation) that is commonly considered small and consequently adopted by multiple simplified approaches (Ferrick, 1985). Both formulations are suitable for supporting the inverse solution for the unsteady flow equations with direct stage measurements at one location.

The first practical form of the reduced Saint-Venant equation is the one proposed by Rátky (2000):

$$Q = Q_0 \sqrt{1 + \frac{1}{c_0 \sqrt{S_s}} \frac{\partial H}{\partial t} - \frac{Q_0}{2Bc_0 S_s} \frac{\partial^2 H}{\partial x^2}} \quad (3)$$

with  $c_0$  a velocity proportional to the reciprocal of the tangent to the steady-state rating determined as  $c_0 \approx \partial Q_0 / \partial A$ , and  $B$  the channel width. The quantity  $S_s$  is determined as  $S_s = S_0 (\partial H / \partial x)$ . This formulation can be used in conjunction with measurements of the free-surface slope at two locations in areas exposed to unsteady flow and/or backwater. The maximum values of the derivatives  $(\partial H / \partial x)$  and  $(\partial H / \partial t)$  are not

simultaneous but they are close, and can be roughly approximated by  $(\partial H/\partial x) \cong -1/c(\partial H/\partial t)$  with  $c$  being the celerity for the depth at time  $t$  (McDonnell & Beven, 2014). With this additional approximation the actual discharge can be determined directly with measurements acquired at one location. Rátky (2000) found that approximative solution based on Equation (3) compares favorably with results obtained with field measurements and numerical solutions applied at actual monitoring sites.

Another useful practical form of the simplified governing equations for non-uniform unsteady flows is developed by Fenton (2001) under the assumption that flood wave propagation is akin to an advection-diffusion process (roughly equivalent to Rátky's formulation). Fenton's formulation encapsulated in Equation (4) was developed to correct an existent steady-state rating with information derived from data acquired at the same site. For wide channels it is assumed that the instantaneous slope of the free surface is expressed in terms of time derivatives of the stage, i.e.,  $(\partial H/\partial x) \cong (\partial H/\partial t)$  which is slightly different than the approximation used by Rátky (2000). Furthermore, assuming that the diffusive terms are relatively small compared with the first term in Equation (1), the unsteady flow discharge can be obtained from:

$$Q = Q_0 \left( 1 + \frac{1}{2} \frac{1}{cS_0} \frac{\partial H}{\partial t} - \frac{1}{2} \frac{D}{c^3 S_0} \frac{\partial^2 H}{\partial x^2} \right) \quad (4)$$

Additional notations to the ones identified above are  $c$  for the wave celerity defined as  $c = 1/B \partial Q_0/\partial H$ , and  $D$  for the diffusion coefficient defined as  $D = Q_0/2B S_0$ . Fenton (2001) states that the above approximations are accurate within 1% if the two diffusive terms are less than 25% from the total sum. The two diffusive terms in the equation are contributing to the budget at different times. The first diffusive term in Equation (4) is important when the stage gradient is high and when the second derivative is small. The second diffusive term is important in the vicinity of the flood peak when the other two terms are small. Results obtained with Equation (4) compares favorably with numerical simulations for a hypothetical site.

Inspection of Equations (1) to (4) reveals that if continuous direct measurements of the flow variables and their spatial-temporal gradients are made with appropriate experimental arrangements, one can use the inverse solution for monitoring of discharge. The steady-state stage-discharge ( $Q_0$ ) in the above equations can be obtained from: a) an existing rating or b) using Equation (2) or similar. If one adopts the first approach, the method can be considered a correction for  $Q_0$  (e.g., Schmidt & Garcia, 2013, and Dottori et al., 2009). If the second approach is adopted, the rating curve can be totally disregarded.

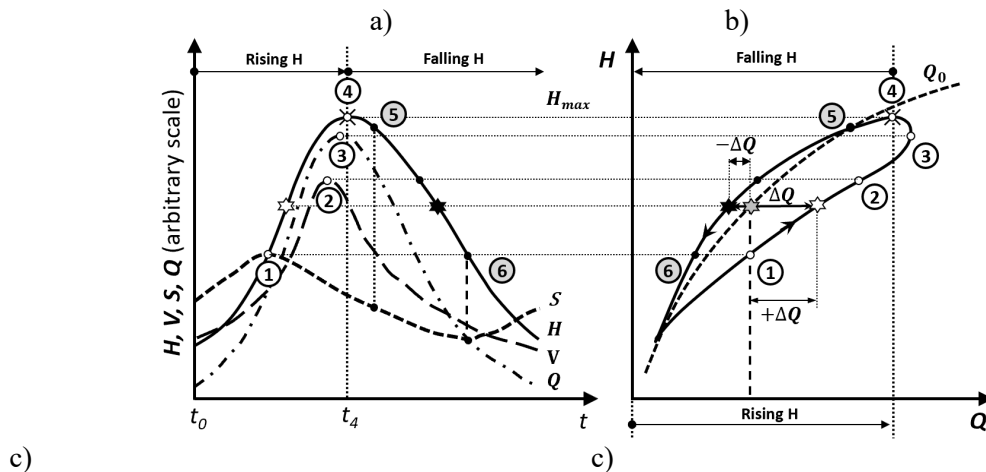
### ***Characterization of hysteretic behavior***

Figure 2 assembles the most relevant conceptual knowledge regarding the behavior of the main hydraulic variables during flood wave propagation as reflected in published studies (e.g., Moots, 1938; Kozák, 1977; Henderson 1966; Rátky, 2000; Graf & Qu, 2004; Muste et al. 2020). For facilitating the descriptions, the solitary wave shapes used for illustrations are intentionally symmetric (i.e., without displaying shorter rising and longer falling legs) and void of potential flow complexities. Given that the actual shapes of the hydrographs are unique for each site and event, their appearance can differ from the conceptual ones depicted in this figure.

Figures 2a-2c illustrate the Eulerian visualization of a solitary flood wave propagation observed over time from a fixed location, a procedure that is commonly used at streamflow monitoring stations. Figure 2a provides the time series for the main hydraulic variables: free-surface slope ( $S$ , positive for  $H_1-H_2 > 0$ ), bulk flow velocity ( $V$ ), stage ( $H$ ) and discharge ( $Q$ ). This visualization substantiates the inter-related gradual changes in the amplitudes and phases occurring on the rising and falling limbs of the flood wave propagation. The phasing of the hydrographs is best tracked by the time lags between their peaks, that inherently occur in the following order: 1)  $S_{max}$ , 2)  $V_{max}$ , 3)  $Q_{max}$ , and 4)  $H_{max}$ . The hydrograph peaks are central to the present analysis hence they are labeled as critical points. Some other critical points (i.e., 5 and 6) reflect properties of the hydrographs derived from analytical geometry considerations. These non-physical arguments are useful in the interpretation of the field data. For example, Henderson (1966, pp. 378-394) demonstrates geometrically that the maximum discharge (point 3 in Figure 2a) is necessarily preceding the maximum depth (point 4 in Figure 2a). The data and information on hydrograph phasing are readily available from numerical simulations of unsteady channel flows but they are peculiarly missing in the in-situ measurements despite their importance for practical applications.

Figure 2b plots the same information as in Figure 2a in time-independent  $H$ - $Q$  coordinates highlighting the critical points of the hysteretic behavior as expected from aggregated knowledge on the process. The figure contains the steady-state stage-discharge relationship to bring about the often-invoked hysteretic loop in the stage-discharge relationships. On the side, it should be noted that such hysteretic loops were captured (possibly for the first time) with direct discharge measurements in the Tisza River acquired from March 23 to May 10, 1895 (Hirschfeld, 1896). These ambitious field campaigns were triggered by the realization that the progression of a flood wave cannot be characterized by only stage measurements, hence direct measurements were acquired to demonstrate the hypothesis. For most of the hydraulic literature hysteresis is synonym with loops around the steady-state HQRC-based rating ( $Q_0$  in Figure 2b) as this approach has been almost exclusively used for monitoring streamflow at gaging stations. Hysteretic loops are however inherent between any two of the hydraulic variables in unsteady flows, as conceptually illustrated in Figure 2c for  $H$ - $V$  and  $H$ - $S$  relationships.

An alternative approach for visualizing the flood wave propagation is the Lagrangian framework shown in Figure 2. This observational perspective, equivalent of two “snapshots” of the propagating wave taken at time  $T_1$  and  $T_2$  from different locations along the stream, enables visualization of instantaneous flood wave profiles and track their deformation during the downstream propagation. Figure 2d, inspired by visualizations by Moots (1938) and Kozák (1977), indicate that each point of the free surface observed at an upstream location can be tracked at a subsequent time at a downstream location (e.g., the point-pair  $1_{t1}$  and  $1_{t2}$  in this figure). Comparison of the two waves indicate a wave deformation (a.k.a. subsidence or attenuation), that is caused by energy dissipation through friction and acceleration of the flood wave (Henderson, 1966). This process is negligible during the propagation of monoclinal kinematic waves, but it is inherent in the propagation of the diffusive solitary waves. The displacement between pairs of homologous points traced in the two-dimensional  $H$ - $x$  plane can be interpreted as vectors resulting from the vectorial sum of a horizontal displacements parallel to the bed slope ( $S_0$ ) and a vertical displacement ( $\Delta h$ ). The horizontal component reflects the horizontal translation of a point of the wave surface driven by the local velocity ( $c$ ) of the wave, a.k.a., wave celerity (Saint-Venant, 1871). The vertical component reflects the deformation (i.e., local rising or sinking) of the free-surface wave that is in turn determined by the nature of the wave (i.e., kinematic, diffusive, or dynamic).



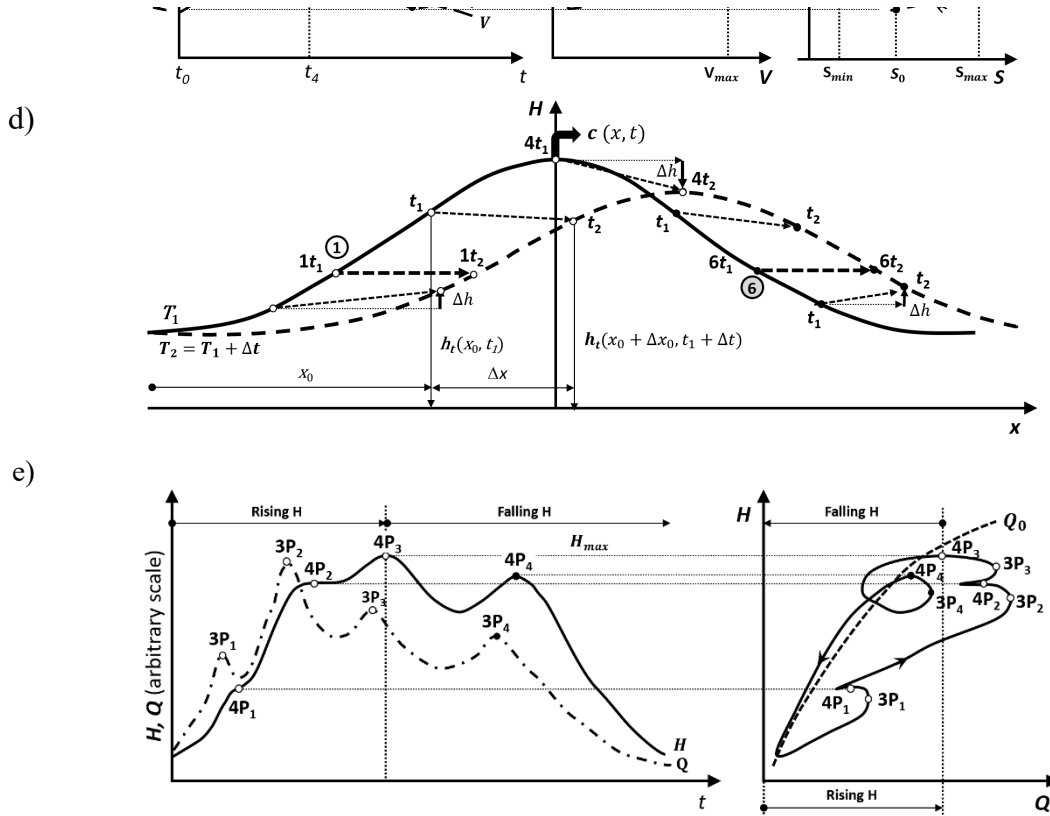


Figure 2. Conceptual knowledge on the hysteretic behavior during the propagation of a flood wave: a) solitary wave phasing; b) stage-discharge relationship; c) stage-velocity and stage-free-surface slope relationship; d) flood wave attenuation; e) multi-pulse wave (train of waves) Notations:  $Q$  – unsteady flow discharge,  $Q_0$  – steady flow discharge and stage-discharge rating (whereby  $S = S_0 = -\Delta z/\Delta x$  with  $\Delta z$  the difference between the bed elevations at two locations spaced at  $\Delta x$  and positive in the downstream direction),  $V$  – cross-sectional velocity,  $H$  – stage (elevation of free surface),  $S = \Delta(H_1 - H_2)/\Delta x$  – positive when  $H_1 > H_2$ ];  $H'_t$  and  $H''_{x^2}$  – first and second derivatives of  $H'$ , respectively;  $\pm\Delta Q$  – discharge difference between steady and unsteady hydrographs;  $c$  – celerity (wave velocity);  $3P_i$  and  $4P_i$  – specific points 3 and 4 in Figures 2a and 1b for peak  $i$  of the multi-pulse series, respectively;  $it_1$  and  $it_2$  – specific points 1, 4.5 and 6 in Figures 2a and 2b at time  $t_1$  and  $t_2$ , respectively.

The graphical representations discussed above highlight valuable insights on multiple hysteretic features, hence underpinning its better understanding. Many of these features can be retrieved from in-situ measurements, as illustrated in the next section. Some of the hysteresis behavior aspects can also be derived based on analytic geometry considerations whereby the change of the variable gradients (ascending or descending lines) and singular points (maximum, minimum, and inflection) can be interpreted from the analytical connections between first and second derivatives of the variable time series. For example, the inflection points 1 and 6 on the rising and falling limbs of the stage hydrograph (an easy-measurable variable) can be correlated with the maximum and minimum points of the free-surface slope (a difficult to measure variable). We point out to this example to highlight that combining knowledge on the hysteresis process with analytic geometry considerations can guide the strategy for acquisition of in-situ data and reveal relationships among variables that are difficult to obtain from measurements. Table 1 summarizes essential features of the hysteretic behavior associated with unsteady flows based on the graphical representations of the process encapsulated in Figures 2a-2d.

Table 1. Essential features of hysteresis behavior during flood wave propagation

Temporal variation of hydraulic variables (Fig. 2a)	Critical points in $H$ - $Q$ representation (Fig. 2b)
$t_0$ : transition from steady to unsteady flow	$t_0$ : $Q = Q_0$ ( $S = S_0$ , = bed slope in steady flow)



$t_0 - t_1$ : free-surface slope increases	$t_1$ : $S_{t1} = S_{max} (H_{x,2}'' = 0, S > S_0)$
$t_0 - t_4$ : rising limb of the stage hydrograph $t_0 - t_2$ : increase of the velocity $t_0 - t_3$ : increase of the discharge $t_1 - t_4$ : decrease of free-surface slope to $S_0$	$t_2$ : $V_{t2} = V_{max} (S > S_0)$ $t_3$ : $Q_{t3} = Q_{max} (Q > Q_0; S > S_0)$ $t_4$ : $H_{t4} = H_{max} (S > S_0)$
$t_4 - t$ : falling limb of the stage hydrograph ( $t_4 - t$ period typically 3-10 times longer than $t_0 - t_4$ ) $t_6 - t$ : free-surface slope increases	$t_5$ : $Q = Q_0 (S = S_0)$ $t_6$ : $S_{t6} = S_{min} (H_{x,2}'' = 0; S < S_0)$ $t$ : $Q = Q_0; S = S_0$
<b>Flood wave attenuation (Fig. 2d) &amp; Rátky (2000)</b>	
Data points under $1_{t1} - 1_{t2}$ and $6_{t1} - 6_{t2}$ are rising	Data points above $1_{t1} - 1_{t2}$ and $6_{t1} - 6_{t2}$ are sinking
Wave attenuation decreases moving downstream	
Wave attenuation increases for larger $\partial H / \partial t$	
Wave attenuation increases for larger roughness if $\partial Q / \partial t \approx const.$	
Wave attenuation increases with higher bed roughness and lower bed slope for $\partial H / \partial t \approx const.$	

The information assembled in Figures 2a-2d and Table 1 expose several important practical considerations, with most of them related to the limited capability of the widely-used steady rating ( $Q_0$ ) to document hysteresis (Henderson, 1966; Fenton, 2001; Rátky, 2000; Muste et al., 2022a, 2022b):

- the peaks of the main hydraulic variables are not simultaneous, rather they are systematically occurring in the following order:  $S_{max}$ ,  $V_{max}$ ,  $Q_{max}$ , and  $H_{max}$ .
- the  $H$ - $Q$  relationship appears as a loop rather than a one-to-one relationship described by the rating developed with steady-state assumption;
- the actual flow discharge ( $Q$ ) is not symmetrically positioned with respect to the uniform and steady rating ( $Q_0$ ). For a given stage, the actual discharge is larger than  $Q_0$  on the rising limb of the hydrograph and closer to  $Q_0$  on the falling limb;
- the actual peak discharge ( $Q_{max}$ ) is always larger than the one indicated by the steady-state rating ( $Q_0$ ) and it arrives before the timing indicated by  $Q_0$ . The difference in discharge values and timing between times  $t_3$  and  $t_5$  is highly dependent of the intensity of the flood wave,  $\partial Q / \partial t$ .
- bulk flow velocities,  $V$ , are larger on the rising limb than on the falling one reaching its maximum before the stage hydrograph;
- $Q = Q_0$  and  $S = S_0$  at times  $t_0$ ,  $t_5$  and  $t$  (at the beginning, around the stage hydrograph peak, and at the end of the base-peak cycling);
- the  $S_{max}$  and  $S_{min}$  values of free-surface slope coincide with the inflection points on the rising and falling limbs of the stage ( $H$ ), respectively. As the streamflow ( $Q$ ) increases, the free-surface slope ( $S$ ) in the stream is larger than the slope in steady flow ( $S_0$ ) at the same stage up to time  $t_1$ . From  $t_1$  to  $t_6$  the free surface slope decreases continuously, while from  $t_6$  to  $t$  increases again; and,
- the maximum free-surface fall (sinking) for the progressing wave occurs between  $t_1$  and  $t_4$ .

The conceptual visualizations in Figures 2a-2d refer to a solitary wave in its simplest form that is rarely (if ever) found in natural streams. Most of the storms appear as multi-pulse waves propagating through the monitoring sites, as illustrated in Figure 2e. Pulses consist of short-time flow “perturbations” superposed on the larger-scale flood wave that cycles from base to peak flow (flood crest) and back. The word “pulse” derives from the hysteresis terminology used in the electrical domain (Henderson, 1966). Flow pulses are generated by changes in precipitation intensity or spatial distribution or by inflows from upstream tributaries entering the stream reach where the gaging is made. While these inflows are reflected in the time series of all the flow variables, illustration is made in Figure 2e for the discharge-stage hydrograph. It can be seen that small inflows during the flood wave progression (denoted by  $3P_i$  in Figure 2e) produce inflection points in the stage on the rising limb (e.g.,  $4P_1$ ,  $4P_2$ ) or a local stage peak on the falling limb (e.g.,  $4P_3$ ,  $4P_4$ ). The maximum value of the stage peaks on the rising limb (a.k.a. flood wave crest) cumulates the impact of all the previous pulses. The plot on the right of Figure 3e displays the actual  $H$ - $Q$  relationship during the wave propagation. The pulse signatures in this plot are visualized by “dents” or smaller

embedded loops in the overall flood wave loop. The actual evolution of the flow discharge is totally missed if a steady-state rating curve is used to determine discharges (see the  $Q_0$  line on the right part of Figure 2e).

### *Anticipating the hysteresis presence*

As mentioned upfront, the presence of hysteresis is not always of concern for practical purposes. Such situations are encountered in streams located on steep slopes where hysteresis is weak. While the information embedded in Figure 2 and Table 1 highlight qualitatively essential features of the hysteretic behavior, the causal relationships determining the magnitudes of the loop thickness and lags among the variable peaks is missing. Efforts to quantify the nature of the flood wave in relationship with the manifestation of hysteresis occurring due to channel storage and flow unsteadiness have preoccupied the scientific community for some time. Such information is critical for informing agencies in charge with the selection of the proper method for each monitoring site and for meaningfully supporting the development of streamflow forecasting models. Lee (2012) identifies 13 methods for quantification of hysteresis diagnostic. In this paper, we use the Mishra & Seth (1996) method which was successfully applied by these authors for several previous case studies.

Mishra & Seth method quantifies the hysteresis severity in terms of change in the hydrological variables. The method can only be applied to past events (post-analysis) at sites where the measured and estimated variables display the hysteretic features illustrated in Figure 2. More specifically, this analysis can be conducted at sites where data from direct discharge measurements, unsteadiness-corrected HQRC, IVRC, or CSA are available. Mishra & Seth classification criterion uses the non-dimensional hysteresis index,  $\eta$ , that is associated with the energy consumed by the wave during its propagation:

$$\eta = \frac{1}{2} \int_0^T \left( q_1 \frac{dh_1}{dt} - h_1 \frac{dq_1}{dt} \right) dt \quad (5)$$

where  $h_1(t) = (H(t) - H_{min}) / (H_{max} - H_{min})$  is the dimensionless stage obtained from direct measurements,  $q_1 = (Q - Q_{min}) / (Q_{max} - Q_{min})$  is the dimensionless discharge obtained with a hysteresis-sensitive tracking methodology, and  $T$  is the total time period for the flood wave cycling. Equation (5) is equivalent with the area of the loop inside the  $h$ - $q$  non-dimensional graphical representation.

Mishra and Seth (1966) also proposed analytical measures for characterization of the wave attenuation described in Figure 2e by introducing the phase difference,  $\varphi$ , between the stage and discharge hydrographs:

$$\varphi = \frac{2\pi}{T} (t_{ph} - t_{pQ}) \quad (6)$$

where  $\varphi$  is in radians,  $t_{ph}$  is the time of rise of the stage ( $t_0$ - $t_4$  in Figure 2a) and  $t_{pQ}$  is the time of rise for the discharge ( $t_0$  to  $t_3$  in Figure 2a). If the stage hydrograph precedes the discharge hydrograph,  $\eta$  is negative.

Mishra & Seth (1996) and Mishra & Singh (2001) tested their parameters with observed and simulated flood events to determine thresholds associated with various types of waves (i.e., kinematic, diffusive, and dynamic). Table 2 assembles their findings.

Table 2. Criteria for wave types (Source: Mishra & Seth, 1996)

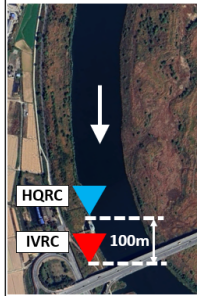

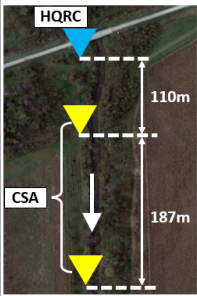

$\eta$ (dimensionless)	$\varphi$ (radians)	Wave type	Hysteresis strength
< 0.025	< 0.03	kinematic	weak
0.025 – 0.1	0.03 – 0.13	diffusive	mild - strong
> 0.1	> 0.13	dynamic	strong

### 3. Experimental evidence substantiating the hysteretic behavior

In the present paper we reveal the hysteresis manifestation over a range of situations using actual measurements acquired during the propagation of different intensity waves occurring at various sites. We do so using visual representations that delineate characteristic features highlighted in Section 2. The traces for stage and index-velocity (or bulk flow velocity) are obtained from publicly available measurements acquired at stations equipped with simple stage-discharge (HQRC) and index-velocity (IVRC) methods (mostly in the US). The traces for the free-surface slope are generated from customized experiments

conducted by the authors or existing experimental arrangements enabling the use of the Continuous Slope-Area (CSA) method. The latter arrangements, currently emerging in the US (Smith et al., 2010), are readily available in South Korea for river reaches displaying complex flows (Kim, 2023). It should be mentioned that the CSA method as applied here is a simplified version of the slope-area method (Dalrymple & Benson, 1967) using data continuously sampled with high frequency (Muste et al., 2019). Table 3 summarizes geometrical and hydraulic characteristics for the sites used in the illustrations along with the measurement methods used for data acquisition.

Table 3. Summary of the site characteristics used for illustration of hysteretic behavior

Site/ River	Naju/ Yeongsan (Korea)	Nampyeong/ Jiseokcheon (Korea)	Oxford/ Clear Creek (IA, USA)	Kingston Mines/ Illinois (IL, USA)
Site view				
$S_0$	0.00025	0.0012	0.00039	0.00002
$B$ (m)	150	140	10	200
$B/h$	36	71	15	80
$Q_{min-max}$ ( $m^3s^{-1}$ )	≈ 526 - 7653	≈ 83 - 738	≈ 1.3 - 25	≈ 219 - 2226

Essential elements of the measurement process for each of the above-mentioned monitoring methods are schematically shown in Figure 3 to inform readers on the measured and estimated data. Details on the HQRC, IVRC, and CSA monitoring methods are available in guidelines of the monitoring agencies (see Section 1) and will be not repeated here. A common feature of the HQRC and IVRC methods is that they use rating curves that are established by concurrent measurements of stage and discharge for HQRC and index-velocity and mean bulk velocity (determined from direct discharge measurements) for IVRC. The measurement results are fit graphically or statistically to yield rating curves under the assumption of step-wise steady flow. As a consequence, the HQRC rating is not perceiving hysteresis at all as the stage is a purely geometric descriptor of the flow. The IVRC and CSA methods add velocity and, respectively, free-surface slope measurements to stage, hence they are better capturing the flow dynamics. Previous streamflow data collected with IVRC and CSA by these authors proved that these methods successfully capture hysteresis in a variety of situations (i.e., Cheng et al., 2019; Lee et al., 2017).

The instruments used for the measurement of hydraulic variables schematically shown in Figure 3 are intrusive (requiring submersion of the probes in the stream). The instruments at the sites presented herein pertain to this family (mostly based on acoustic technology) that is widely used at modern gaging station worldwide. It should be mentioned that today, stream monitoring is increasingly approached with novel and innovative alternative instruments and deployments. There is a plethora of new generation of instruments for stage and velocity measurements based on lidar, radar, and image-based principles that can be deployed at close range, installed on drones, or remote-sensing the river from airplanes or satellites (Paul et al., 2020; Bandini et al., 2021; Ho et al., 2022; and Yoshida et al., 2023). For reliable extraction of hysteretic behavior is desirable to use instruments of high accuracy and high-frequency sampling rates deployed from stable and precisely identified locations. Long-term repeated measurements supported with by real-time data transmission for rapid interventions in cases of failures are considered necessary.

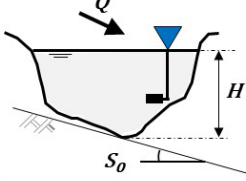
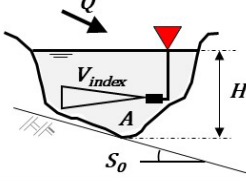
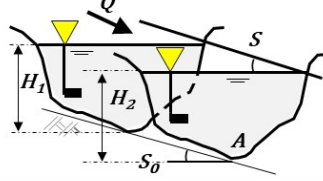
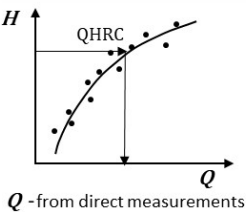
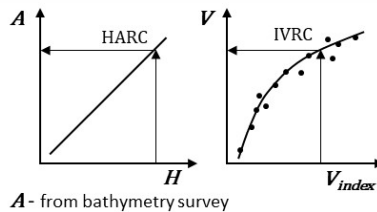
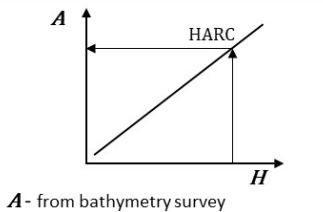
Method/ Specifications	Stage-discharge method (HQRC)	Index-velocity method (IVRC)	Continuous slope-area (CSA)
Continuously measured	Surface stage, $H$ (one location)	Surface stage, $H$ ; Index-velocity, $V_{index}$ (one location)	Free-surface slope, $S$ (two locations)
Experimental arrangement			
Supporting rating(s)	 $Q$ - from direct measurements	 $A$ - from bathymetry survey $V = Q/A$ ; $Q$ from direct measurements	 $A$ - from bathymetry survey
$Q$ estimation	$H \rightarrow \text{QHRC} \rightarrow Q$	$H \rightarrow \text{HARC} \rightarrow A$ $V_{index} \rightarrow \text{IVRC} \rightarrow Q = A \cdot V$	$Q = 1/n AR^{2/3} S^{1/2}$ (SI units)

Figure 3. Summary of the measurement flux for conventional streamflow monitoring methods.

The first illustration of the hysteretic behavior is provided in Figure 4 with data acquired for the IVRC and CSA methods at Naju gaging station #5004550 on the Yeongsan River in Korea (<http://www.yeongsanriver.go.kr>). This is the only station in our illustrations that can provide direct measurements for all the hydraulic variables discussed in the conceptual sketches of Section 2. Stages for the HQRC station are measured with Level TROLL 400 Data Logger (<https://in-situ.com/us/level-troll-400-data-logger>). Stages and index velocities serving the IVRC station are measured with a SonTek SL500 Side-Looking Doppler Current Meter (<https://www.xylen.com/en-us/products>). The local free-surface slope is determined from the stage measurements at the HQRC and IVRC stations located 100-m apart. All instruments are synchronized to acquire data every 10 minutes.

An inherent difficulty in analyzing data acquired in situ is the “noisy” mature of the raw signals of the variables generated by natural flow perturbations and errors accumulated through the measurement process. The level of noise is not uniform across variables. The lowest level is in the measurement of stage and higher degrees of noise can be seen in the index-velocity measurements and free-surface velocity records. The free-surface slope data display the largest noise level because, on one hand, their values are small when determined from stage measurements over short distances (in this case 100 m) and, on the other hand, the free surface fluctuates sensibly due to natural causes (large-scale turbulence in the water body and wind action at the surface). Practical guidelines recommend that slope measurements should be determined from falls of about 0.25-0.3 m, which was not the situation for the present case. The noisiness of the signals hampers the accurate identification of the magnitude and timing of the hydrographs especially near their peaks. In order to limit the noise impact on the signal analysis, a 5-point moving average was uniformly applied for this, and, all other raw datasets discussed in the present paper. This method was found adequate when compared to other 18 often-used smoothing alternatives (Baydaroglu et al., 2024).

The variable traces illustrated in Figures 4a-4d show that both IVRC and CSA method reveal the overall trends expected by the hysteresis presence (see Figures 2a-2d). Relationships for the variables are reported for the IVRC cross-section. The time lags between the peak of the free-surface slope and index velocity and the peak of the stage hydrograph are of the order of several hours for this case. The discharge,  $Q$ , in Figure 4a is estimated with the IVRC method. The maximum loop thickness in Figure 4b is  $1,448 \text{ m}^3\text{s}^{-1}$  representing 36% from the smaller discharge value at the stage indicated in the figure. Due to the noisiness of the signals, we only show the critical points 1,2,3, and 4 in Figures 4a-4d leaving aside the critical points 5 and 6 shown in Figures 2a and 2b. Figures 4e and 4f, illustrate the discharges computed with inverse

solutions using Equations (3) and (4) along with the discharges estimated with Manning' Equation (2) and the IVRC method. Equation (1) cannot be used as we do not have direct measurements for the gradient velocity,  $(\partial V/\partial x)$  and  $(\partial V/\partial t)$ . Given the approximations involved in Equations (2), (3), and (4), we deem that the appropriate reference for the comparison is the discharge obtained with the IVRC method. The inverse solutions for Equations (3) and (4) reveal that the discharge arrives sooner than the steady discharge,  $Q_0$ , as expected. There are loops associated for Equations (3) and (4) in Figure 3f, but they are slightly narrower than IVRC, which is also expected as these equations neglect the local acceleration term in Equation (1). Still the magnitudes of the hysteresis loop with respect to steady-HAQRC at the indicated stage are 11%, 15%, and 33% for the discharges estimated with Equation (3), Equation (4), and IVRC method, respectively.

Figure 4g tracks the fluvial wave propagation between the Naju IVRC station indicated in Table 3 and an HQRC station located 5,753m downstream on Yeongsan River. The wave "snapshots" were analytically determined using the following algorithm:

- a) Calculate  $\partial H/\partial t$  from the hydrograph  $H(t)$  measured at the upstream observation point. The snapshot of the flood wave when it has completely passed through this observation point is denoted as  $T_1$ .
- b) Determine the wave celerity,  $c = 3/2 V$ , corresponding to the time of the wave passing through the upstream observation point. Using the determined  $c$  and  $\partial H/\partial t$  time series, calculate  $\partial H/\partial x$  from the  $\partial H/\partial x = -1/c \partial H/\partial t$  relationship for each successive sampling time at the upstream station. Determine the incremental wave displacements in the horizontal direction using  $\partial x = \partial t/c$ .
- c) Determine the wave shape  $H(x)$  at  $T_1$  by integrating  $\partial H/\partial x$  using the incremental displacements calculated in step b). Determine the wave shape  $H(x)$  progression in the downstream direction during time  $\Delta t = T_2 - T_1$ . as  $\Delta x = \Delta t c$ , Determine the wave shape progression in the vertical direction,  $\Delta H$ , assuming  $\partial H/\partial x = \Delta H/\Delta x$ , to obtain the fall/rising of the wave at time  $T_2$ .

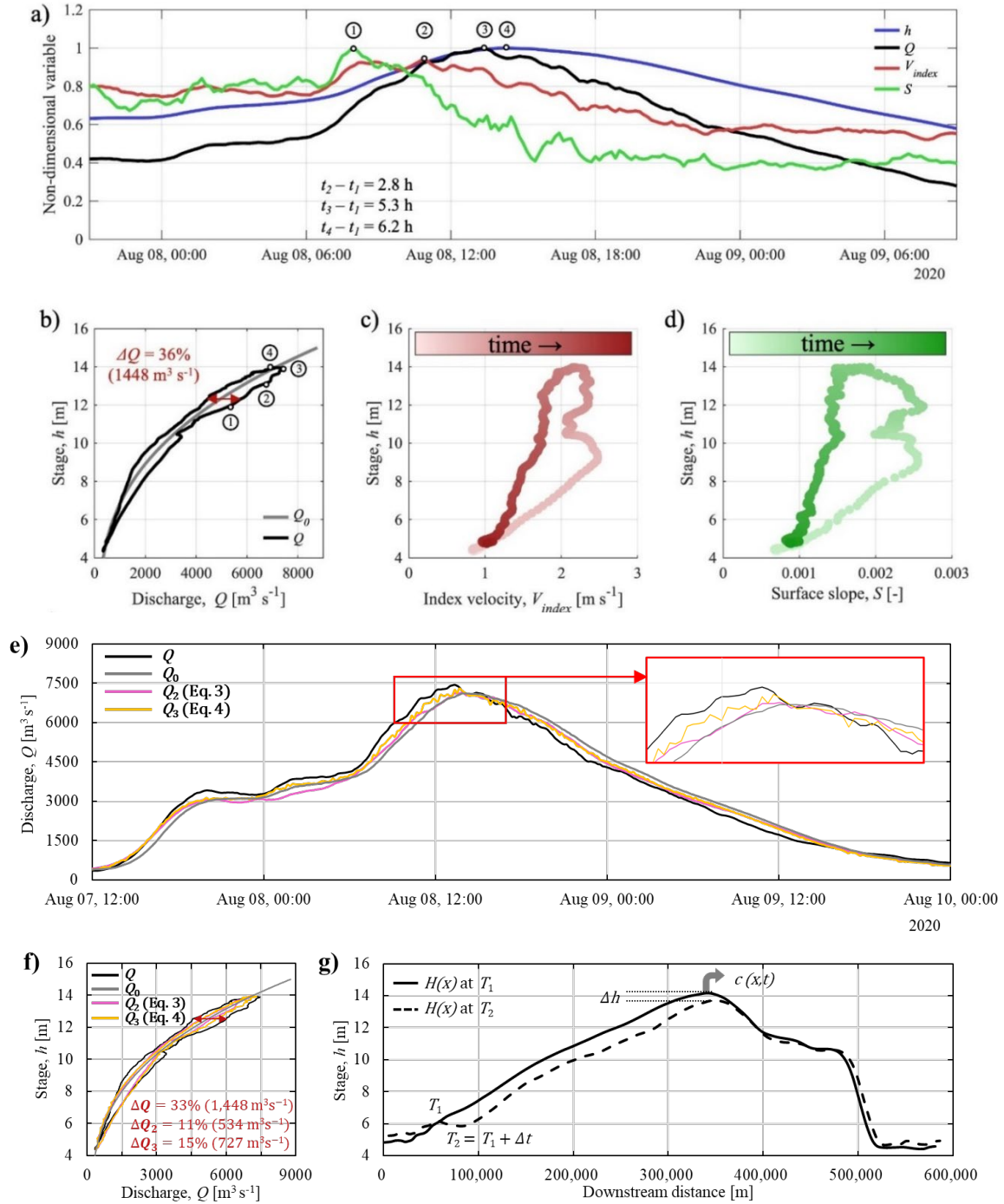


Figure 4. Relationships among hydraulic variables measured and estimated with the HQRC-IVRC-CSA methods deployed at a gaging site on Yeongsan River ((#5004550) for the event with  $Q_{max}$ :  $7,653 \text{ m}^3 \text{ s}^{-1}$ ;  $h_{max}$ :  $14 \text{ m}$ ;  $V_{max}$ :  $2.5 \text{ ms}^{-1}$ ;  $S_{max}$ :  $0.0027$ : a) Temporal variation of the variables; b) hysteresis plotted in the  $H-Q$  coordinates; c) hysteresis plotted in the  $H-V_{index}$  coordinates; d) hysteresis plotted in the  $H-S$  coordinates; and e) discharge time series obtained with equation (2), IVRC method, and Equations (3) and (4); g) discharges in Figure 3e plotted in  $H-Q$  coordinates; g) wave attenuation during the flood wave propagation through the site,  $c = 2.90 \text{ ms}^{-1}$ ,  $\Delta h = 0.64 \text{ m}$ ,  $\Delta t = 28 \text{ min}$ ,  $\Delta x = 5,753 \text{ m}$ . The arrow on the color gradients in Figure 5c indicates the time sequence for data acquisition.



The second sample of direct measurements for substantiating the hysteretic behavior conceptually sketched in Figures 2a-2c is visualized in Figure 5 with data acquired every 15 minutes for the IVRC method at the USGS gaging station #05568500 on Illinois River. The plotted time series are public data reported on the stream gaging website (<https://waterdata.usgs.gov/nwis>). The index-velocity data is acquired with a SonTek SL500 Side-Looking Doppler Current Meter (<https://www.xytem.com/en-us/products>). The stage data is acquired with a Design Analysis WaterLog H350 pressure sensor (<http://www.ysi.com>). Note that temporal variation for the variables in Figure 5a do not end at the same values. This is because immediately after the storm event illustrated in the figure another one was initiated. Situations whereby the storm events are not fully cycling base-to-base are common in natural streams due to changes in the precipitation spatial-temporal distribution in the drainage basin leading to the station.

Figures 5a-5c display the stage data recorded by the pressure sensor, the index-velocity measured by the HADCP, and the discharge determined with the IVRC method. There is no HQRC available for this site. For completeness of the illustration, we constructed a surrogate HQRC rating, shown in Figure 5b, using the calibration data acquired for building the  $V_{index}$ - $V_{mean}$  rating curve. While the free-surface slope is not available from direct measurements, it could have been added for completeness using the surrogate  $dh/dx \sim 1/c dh/dt$  approximation used by Rátky (2000). However, we intentionally omit this variable from the illustration to not influence the analysis with approximations. Consequently, the only critical points indicated in Figure 5a are 2, 3, and 4. Notable in Figures 5a and 5b is the large time lag between the variable peaks (i.e., one order of magnitude larger than in Figure 4a) despite that the loop thickness is of the same order of magnitude, i.e.,  $\Delta Q = 41\%$ . The large difference between the index-velocity and stage peak lag of 3.6 hours in Yeongsan River compared to the 82 hours (equivalent of 3.4 days!) in Illinois River can be attributed to the flashier nature of the first river (see also Figures 8 and 9 below).

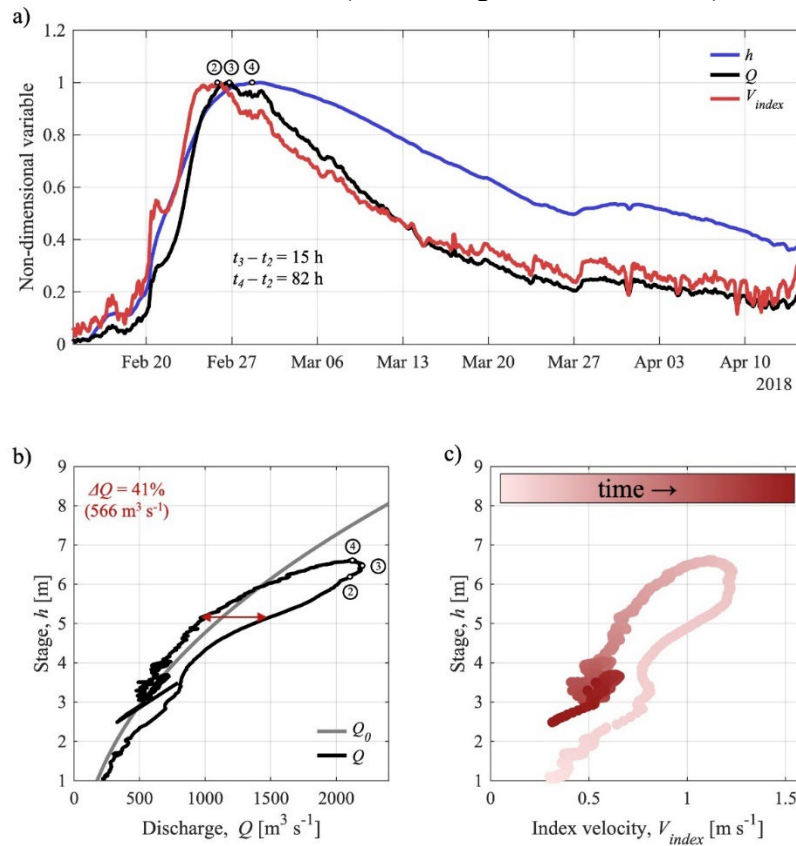


Figure 5. Relationships among hydraulic variables measured and estimated at the IVRC gaging site on Illinois River (USGS #05568500) for the event with  $Q_{max}$ : 2,220  $m^3 s^{-1}$ ;  $H_{max}$ : 6.8 m;  $V_{max}$ : 1.24  $m s^{-1}$ : a) Temporal variation of the variables; b) hysteresis plotted in  $H$ - $Q$  coordinates; and c) hysteresis plotted in

$H$ - $V_{index}$  coordinates. The arrow on the color gradients in Figure 5c indicates the time sequence for data acquisition.

Figure 6 reinforces and complements the illustrations in Figures 4 and 5 with a set of measurements acquired 15 minutes apart with CSA and HQRC at the USGS gaging station #05542020 on Clear Creek. The HQRC method is supplied with stage measurements acquired with an Amazon150-1-00-0 15 PSI pressure sensor (<https://www.ysi.com/amazon>) The stage data for the determination of the free-surface slope is obtained with pressure sensors embedded in the SonTek-IQ vertical velocity profilers (<https://info.xytem.com/sontek-iq-manual.html>). The discharge data obtained with CSA method are plotted by the  $Q$  line in Figures 6a and 6b and compared with the USGS steady HQRC rating,  $Q_0$ . The discharge data obtained with HQRC method is plotted in Figure 6b. From reasons mentioned above, we do not consider the mean velocity trace in this figure that can be indirectly determined using the discharges offered by HQRC or CSA methods. The time lag between the slope and depth peaks is the smallest of all the illustrated datasets, i.e., 1.5 hours. However, the loop thickness indicated in Figure 6b is on par with the other cases, i.e.,  $\Delta Q = 50\%$  ( $6.4 \text{ m}^3\text{s}^{-1}$ ), a percentage difference that might be surprising given that the stream is quite small (the smallest from all presented cases). Added to the plots in Figures 6a and 6b are the critical points 1, 3, and 4 as they are based on only directly measured or estimated quantities.

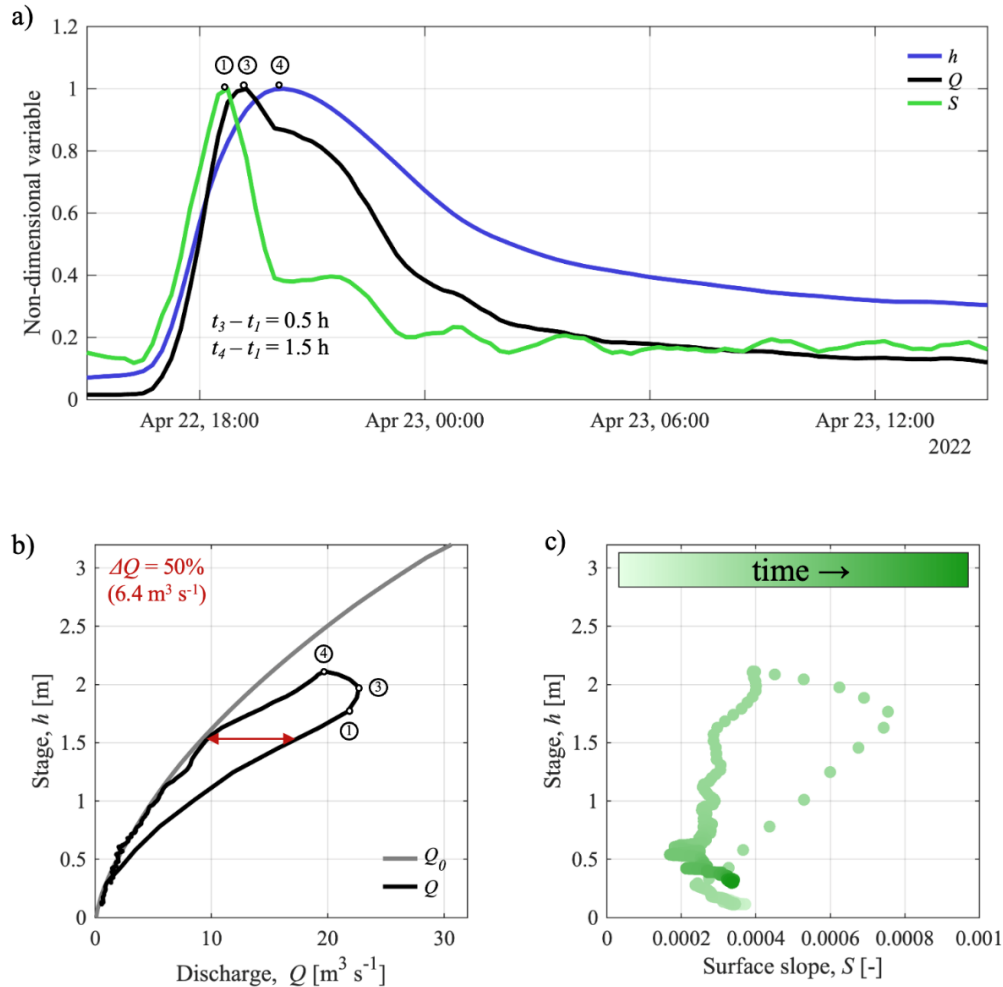


Figure 6. Relationships among hydraulic variables measured and estimated at the CSA gaging site on Clear Creek (USGS #05454220) for the event with  $Q_{max}$ :  $24.7 \text{ m}^3\text{s}^{-1}$ ;  $H_{max}$ : 2 m;  $S_{max}$ : 0.0007: a) Temporal variation of the variables; b) hysteresis plotted in the  $H$ - $Q$  coordinates; c) hysteresis plotted in the  $H$ - $S$  coordinates. The scale of the color gradients in Figure 5c indicates the time sequence for data acquisition.



An additional illustration is provided in Figure 7 for a multi-pulse storm event propagating through the USGS gaging station #05568500 on Illinois River. The traces of the variables shown in Figure 7a enable to observe that the phasing of the variables is maintained for each pulse, albeit in a less apparent manner given that the first two pulses at the bottom of the rising limb are of small intensity for this event. The superposition of the loops associated with individual pulses on the overall flood wave loop are substantiated in the bivariate representations of Figures 7b and 7c where multiple “kinks” are visible in the overall loop compared with a single-pulse event at the same station (see Figure 5c).

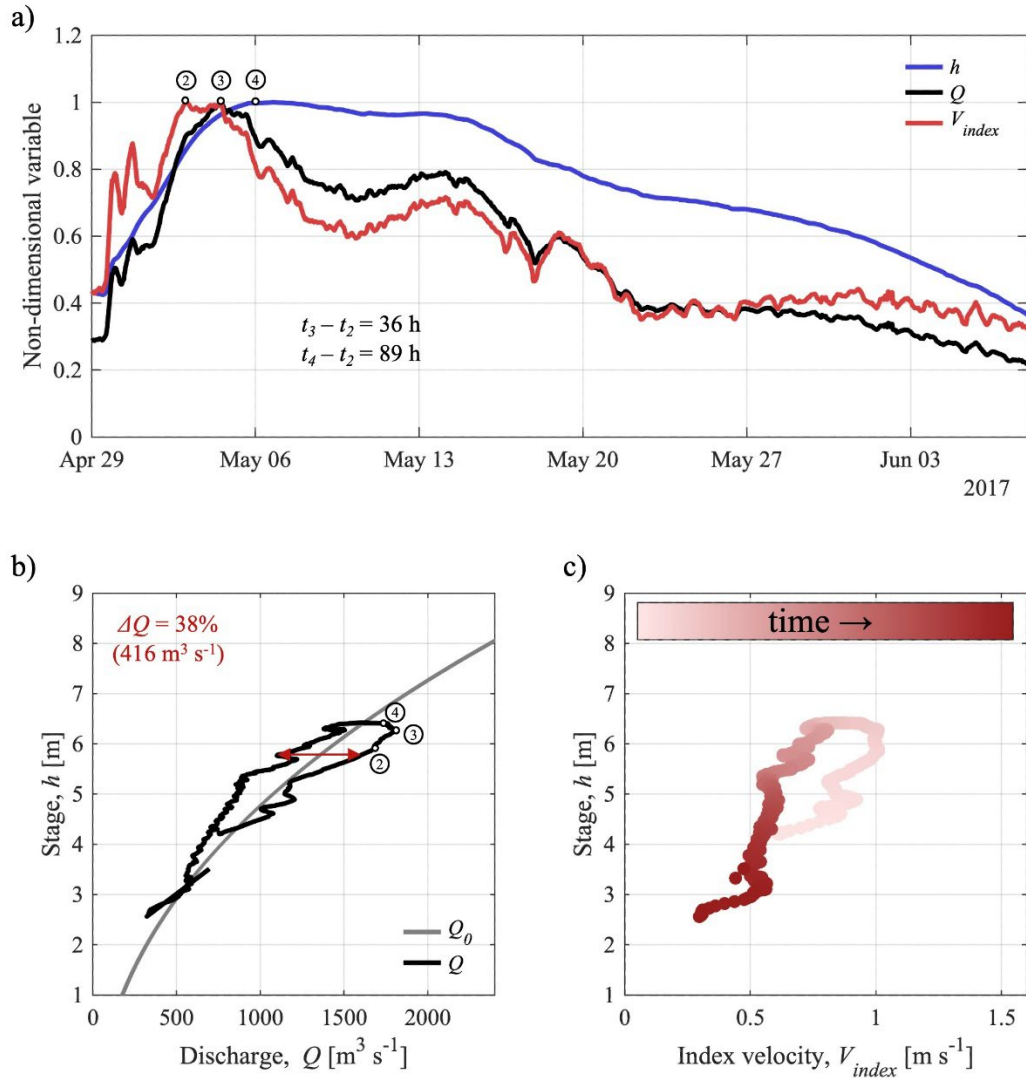


Figure 7. Relationships among hydraulic variables measured and estimated at the IVRC gaging site on Illinois River (USGS #05568500) for a multi-pulse storm event with  $Q_{max}$ :  $1,832 m^3 s^{-1}$ ;  $H_{max}$ : 6.4 m;  $V_{max}$ :  $1.02 m s^{-1}$ : a) Temporal variation of the variables; b) hysteresis plotted in the  $H$ - $Q$  coordinates; and c) hysteresis plotted in the  $H$ - $V_{index}$  coordinates. The arrow on the color gradients in Figure 5c indicates the time sequence for data acquisition.

The experimental evidence in Figures 4, 5, and 6 illustrate ranges for the magnitude of the phase lags in the variable hydrographs and for the loops widths as determined from direct measurements of the stage, index-velocity, and free-surface slope during the largest event in the recorded data for the reference period considered at each gaging station. The illustration shown below are for three different event intensities occurring at the same site to substantiate the sensitivity of hysteresis to the event magnitude. A useful

exercise would be to relate the visual appearance of the measured variables with generic qualifiers of the individual storms using non-dimensional measures that can substantiate the type of waves developed for each storm. Figures 8, 9, and 10 make recourse to the Mishra & Seth (1996) hysteresis diagnostic formulas to link the visual appearance of the hysteresis in time-dependent and time-independent coordinates with the nature of the propagating waves. The plots in these figures refer to storms of different intensities occurring at Naju, Nampyeong, and Kingston Mines gaging sites (see Figure 3).

To highlight the impact of the intensities of individual storms propagating at each site, we pair the Mishra & Seth non-dimensional plots with dimensional  $H-Q$  representations of the same storms. It should be noted that the quality of the HQRC ratings is not certain for the high-flow area as they are developed using a much smaller sample of direct measurements compared with the lower flow range. Figure 8 presents this comparison for three storms at the Naju gaging station on Yeongsan River (Korea). Figures 9 and 10 illustrate the same comparisons for three intensity storms passing through Kingston Mines station on Illinois River and Nampyeong #5003680 station on Jiseongchong River <http://www.yeongsanriver.go.kr>, respectively. The Nampyeong site, characterized in Table 2, is included in the illustration as it is located on the steepest bed slope of all sites analyzed here. An important observation is that the hysteretic behavior is visible in all the cases even if the bed slope at the sites varies over two orders of magnitude.

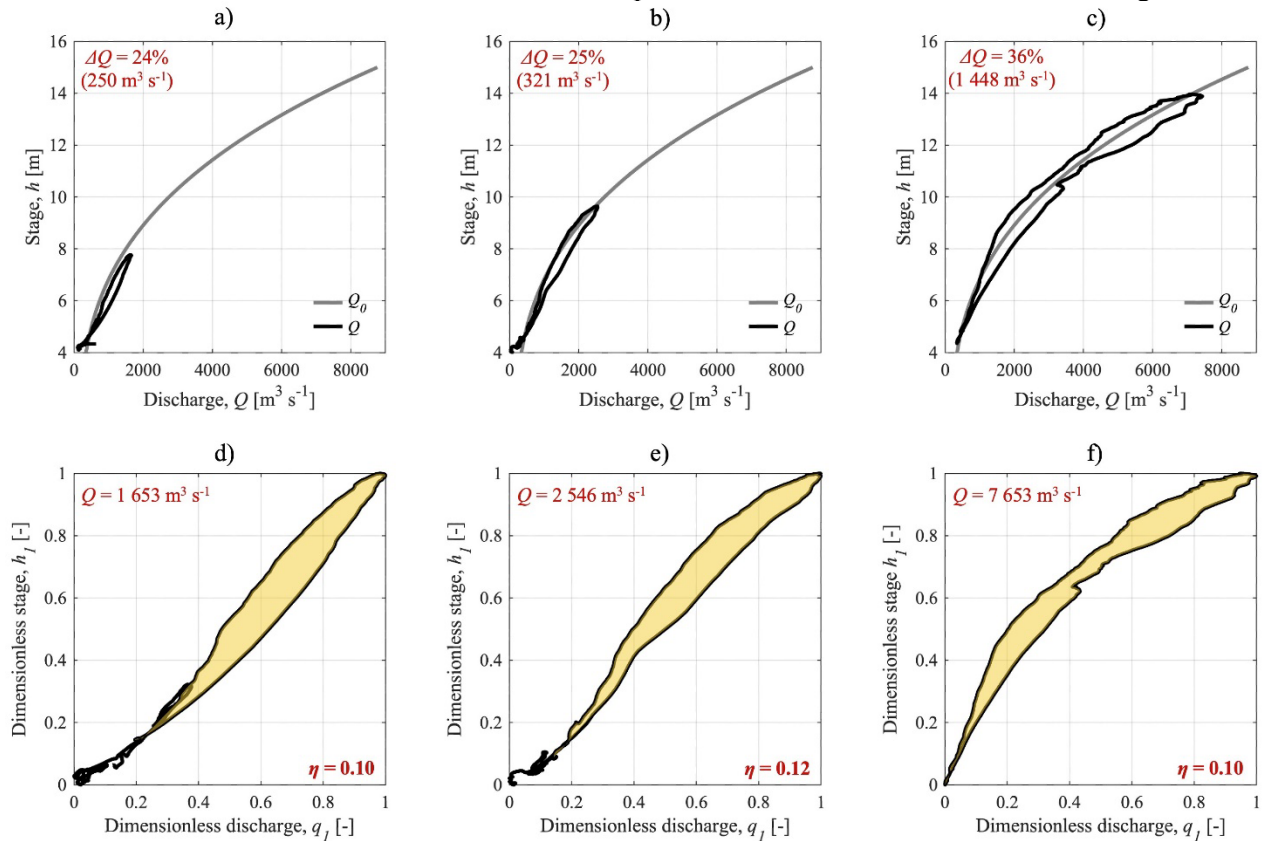


Figure 8. Dimensional and non-dimensional representations of three different storm intensities recorded at the Naju station. Maximum discharges for the three events: 1,653, 2,546, and 7,653  $\text{m}^3 \text{ s}^{-1}$ : a), b), and c) actual flows ( $Q$ ) compared with the those indicated by the steady-state rating curve ( $Q_0$ ); d), e), and f) representation of the storms above in non-dimensional  $h-q$  Mishra & Seth formulation.

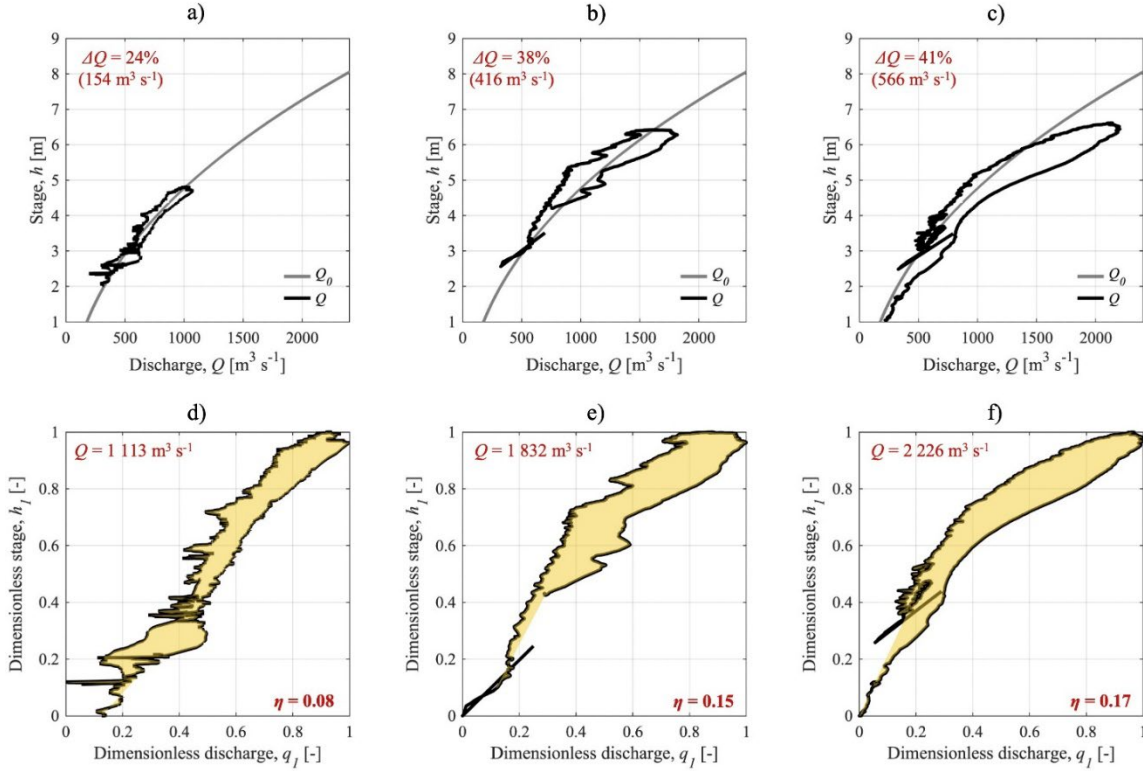


Figure 9. Dimensional and non-dimensional representations of three different storm intensities recorded at the Kingston Mines station. Maximum discharges for the three events: 1,113, 1,832, and 2,226  $\text{m}^3\text{s}^{-1}$ ; a), b), and c) actual flows ( $Q$ ) compared with those indicated by the steady-state rating curve ( $Q_0$ ); d), e), and f) representation of the storms above in non-dimensional  $h$ - $q$  Mishra & Seth formulation.

The results of the analysis of these nine events using quantitative estimators  $\eta$  and  $\phi$  defined by Equations (5) and (6), respectively, are listed in Table 4. The numerical values for the two parameters in Table 4 for each event analyzed in Figures 8, 9 and 10 are in good agreement with those in Table 2 where association is made between threshold values and various types of waves. The qualifiers for the severity of hysteresis specified in the last columns of Tables 2 and 4 are not based on rigorous criteria; rather they are judged by the present authors based on the experiences with the process. It is obvious that a more robust method for assessing the severity of hysteresis is needed as these qualifiers are perhaps the most important pieces of information to convey to the general public when using the analysis for preparing flood warnings.

The qualitative and quantitative qualifiers in Table 4 confirm that the type of wave and severity of hysteresis depend on the combined effects of storm intensity and the slope of the bed at the site (Perret et al., 2022). It can be noticed that the  $\eta$  parameter increases gradually from kinematic to diffusive and dynamic waves for the same site and the  $\eta$  parameter values are larger for all storms propagating in lower bed slopes. This inverse dependence is well illustrated by the average severity estimated across the three storm events analyzed for each site. Specifically, strong hysteresis is found at Kingston Mines station where the slope is 0.00002, mild severity at Naju station where the bed slope is 0.0025, and weak severity at Nampyeong station where the slope is 0.012. This clear delineation of the hysteresis severity is obviously driven by the difference in the order of magnitude of the bed slopes at the three selected sites. We conclude that the results shown in Figures 8, 9 and 10 are encouraging for hysteresis diagnostic purposes as using objective criteria we get to outcomes predicted by theoretical considerations. We are aware though that a more committed and analytic approach is needed to obtain trustworthy and generalizable inferences.

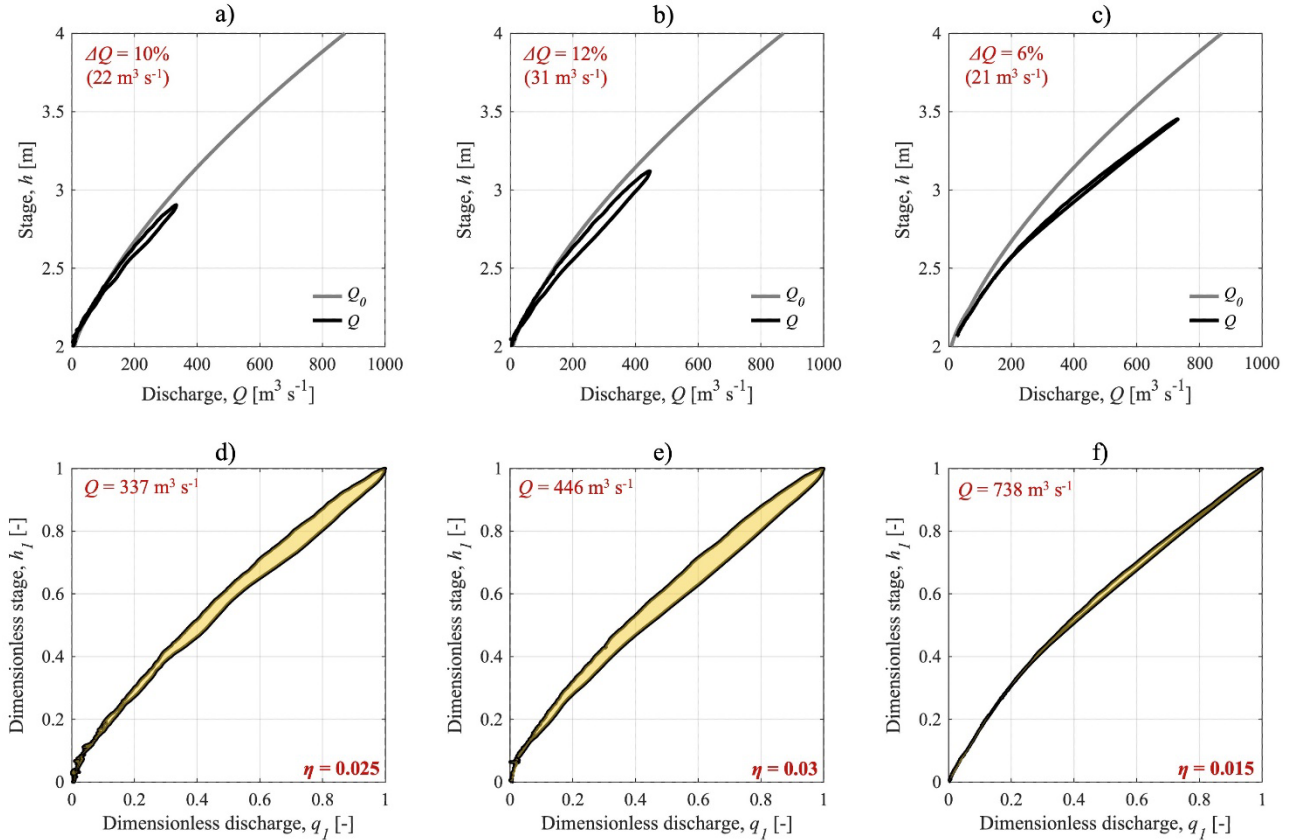


Figure 10. Dimensional and non-dimensional representations of three different storm intensities recorded at the Nampyeong station (Korea). Maximum discharges for the three events: 337, 446, and 738  $\text{m}^3\text{s}^{-1}$ : a), b), and c) – actual flows ( $Q$ ) compared with those indicated by the steady-state rating curve ( $Q_0$ ); d), e), and f) representation of the storms above in non-dimensional  $h$ - $q$  Mishra & Seth formulation.

Table 4. Application of Mishra & Seth (1996) diagnostic criterion to observed flood wave events

Site & event (illustration)	$\eta$	$\phi$ (radians)	Wave type	Hysteresis severity	
				$\Delta Q$ (%)	Category
Naju (Fig. 8a)	0.1	0.10	diffusive	24	mild-weak
Naju (Fig. 8b)	0.12	0.14	dynamic	25	strong
Naju (Fig. 8c)	0.1	0.08	diffusive	36	mild-strong
Kingston Mines (Fig. 9a)	0.08	0.32	diffusive	25	mild-strong
Kingston Mines (Fig. 9b)	0.15	0.30	dynamic	38	strong
Kingston Mines (Fig. 9c)	0.17	0.33	dynamic	41	strong
Nampyeong (Fig. 10a)	0.025	0.01	kinematic	10	weak-mild
Nampyeong (Fig. 10b)	0.03	0.02	kinematic	12	weak-mild
Nampyeong (Fig. 10c)	0.015	0.01	kinematic	6	weak

#### 4. Discussion

During the century-long period of acquiring in-situ measurements in rivers, the issue of capturing relationships among hydraulic variables during fluvial wave propagation has received much less attention compared to the monitoring of flow rates that are of primary interest for multiple uses. The exploration of the basic relationships among hydraulic variables is the first needed step to develop robust, physics-based

protocols for streamflow monitoring. Lacking a full understanding of the mechanisms underpinning the non-unique relationships between pairs of hydraulic variables during unsteady flow events, the monitoring methods have been initially developed using a stepwise steady-state assumption for estimating the discharge. While these methods have been commonly applied to estimate discharges at the worldwide stations for over a century, they have achieved only a limited degree of success because of simplifying assumptions on the flow hydrodynamics. The understanding of hysteretic behavior is still incomplete today, hence the re-examination of the underlying physics of unsteady nonuniform flows remains a priority for improving the monitoring and modeling of these flows for practical and scientific purposes.

The conceptual and experimental evidence assembled in this paper highlights the multi-faceted manifestations of the hysteresis behavior and its pervasiveness in natural streams. These illustrations are especially relevant for the frequent changes in channel storage and unsteady flows occurring during the water movement in lowland and plain waterways. The evidence clearly shows that while the current practice of determining discharges from measured stages and stage-discharge rating (HQRC) relations is reasonable for steady flows, problems with these ratings are inherent when used in unsteady flows. For long time, the loop in stage-discharge relationship has been considered the only perceptible effect of hysteresis in open-channel studies. Illustrations of data provided by the IVRC and CSA methods indicate that they capture hysteretic features in the directly measured variables including the rarely reported phasing of the hydrographs during fluvial wave propagation. The main contribution of this paper is in summarizing the current state of knowledge on the intricate relationships among the primary hydraulic variables and pairing the expected trends with in-situ data collected with other than HQRC data streams. Another contribution of the paper is to reveal that a theoretical-, rather than empirical-based approach can be used for continuous streamflow monitoring that is exclusively relying on direct measurements of hydraulic variables and their gradients without making recourse to ratings or empirical adjustments that are not physically justifiable.

The type of investigation conducted herein is complementary to the few studies conducted in natural open-channel unsteady flows. For example, Arico et al. (2009) verified a newly developed flood routing solver based on sporadic free-surface measurements; Smith et al. (2010) tested an experimental arrangement to test the slope-area method for estimation of streamflow in ephemeral streams; Rowinski et al. (2000) and Mrokowska et al. (2015) measured free-surface slopes to determine shear velocities; Gunawan (2010) used data collected with a customized system to assess the vegetation impact on flow resistance, and Ho et al. (2022) measuring free surface slope with radar sensors. To the knowledge of these authors, the present and some of our previous studies (i.e., Muste et al., 2019; Muste et al., 2020; and Muste et al., 2022b) are the rare (if not the only) systematic analyses on the capabilities of the newer monitoring methods to capture hysteretic loops and phasing of hydraulic variable progression during flood wave propagation. From this perspective, it is desirable to extend the detailed analysis presented on the HQRC stage-discharge relationship (see Figures 2a, 2b, 4, 5, and 6) to IVRC and CSA methods. Also essential for systematic studies is to generalize the hysteresis analysis in conjunction with hydrological drivers such as the shape of the hydrographs (e.g., Zuecco et al., 2015; Lloyd et al., 2016) and the geo-morphological characteristics of the catchments (e.g., Haddadchi & Hicks, 2021).

The importance for continuing and accelerating the understudied effects of hysteresis is highlighted by the ample sizes of the hysteretic loops illustrated in Figures 4a, 5a, and 6a and the data in Table 4. Differences up to 65% in the loops for the same stage of were found in a study of the authors at another site on Illinois River (Muste et al., 2022). The present comparisons of the HQRC data with those provided by IVRC, and CSA measurements in unsteady flows are by far above the desirable 5% uncertainty in the discharge measurements generally accepted for medium to large river sizes by management agencies (Levesque & Oberg, 2012). The reported differences are also above the uncertainties of 6% to 19% range found in small rivers where the noise in the measured signals is further increased (Harmel et al., 2006). The type of uncertainty introduced by the HQRC method is labeled as epistemic by Schmidt (2002) as it is generated by ill-posed assumptions in the monitoring approach. Accepting large epistemic uncertainties becomes a source of “noise” in itself as they are always augmented by other error sources inherent in measurements and multiple other sources of errors in hydroclimatic data when measurements are used for hydrological modeling or streamflow forecasting (Thébault et al., 2023). Unfortunately, currently,



forecasting models are only assimilating stage and HQRC discharge. Making proper arrangements to assimilate the index velocity and/or free surface slope measurements provided by IVRC and CSA methods into physically-based hydrologic models can improve their accuracy bringing about substantial benefits for the short-term streamflow forecasting.

The experimental evidence presented in this paper shows that HQRC data in highly dynamic flood waves could significantly underestimate the peak discharge (4b, 5b, and 6b) and erroneously estimate the arrival time of the peak discharge and stage (4a, 5a, and 6a) that in turn has detrimental consequences in supporting models for flood warning predictions. Similarly, ignoring differences between instantaneous discharge and its time integral provided by steady-state monitoring (e.g., single-valued HQRC ratings) and more dynamic ones (e.g., IVRC and CSA) could impact the estimation of the water-quality constituent loads (suspended or dissolved) and assessing the flow dynamic impacts on the river ecosystem (Kämäri, et al., 2018). While not presented in this paper, it should be mentioned that the vast majority of studies reporting sediment-flow hysteresis (e.g., De Sutter et al., 2001; Gao & Josefson, 2012; Gellis, 2013; Liu et al., 2023) are using the simple stage-discharge rating that is itself affected by hysteresis. It is therefore apparent that calculations of sediment load for suspended sediment (or any other matter in suspension) transported during unsteady flow with steady-state HQRC are inaccurate. From this perspective, it is apparent that continuing river monitoring with HQRC that completely ignores hysteresis is hardly appropriate for managing water issues or conducting scientific investigations during shorter- or longer-duration flow transients. Switching to more precise monitoring approaches such as IVRC and CSA have to be intensified for unsteady flow situations where accurate peak and integral flow values are needed, or high data uncertainties are of concern.

It is deemed that intensifying the hysteresis exploration with new measurement approaches akin to IVRC and CSA (e.g., Ho et al, 2022) contributes to better understanding of unsteady flows and opens research venues that can enhance the quality of in-situ measurements and of the hydraulic & hydraulic models used for water resources management and streamflow forecasting. The last assertion stems from the perception that currently modeling is more focused on developing new methods for integrating the differential equations, rather than to attack the basic equations with new approaches (Yevdjovich, 1964). The need for new measurement approaches is also desirable for improving the accuracy of numerical modeling in analyzing realistic flows. This need stems from the fact that the closer the numerical treatment to the actual channel conditions, the more complex becomes the relationship between variables, and the greater is the necessity for more data describing the channel and the true variable hydrograph. To change the paradigm, we need good-quality in situ data collected with multivariate monitoring approaches that are mined by customized machine learning (ML) tools capable to extract trends and singular points with physical significance for hysteretic behavior (Feng et al., 2020). There are ample opportunities to use sophisticated ML approaches that consider multiple variables and cast the entire methodology into a probabilistic framework rather than a deterministic one. Given the above-mentioned considerations, we believe that use of good quality situ-data acquired in well understood measurement conditions in conjunction artificial intelligence guided by physical principles is perhaps the fastest path toward advancing our knowledge about hysteresis and its possible characterization compared to insights obtained from theoretical investigations or numerical simulations.

Fortunately, the recent advancements in measurement technologies open possibilities to tackle inverse solutions for Saint-Venant equations with the variables and gradients required in Equation (1) determined from direct measurements with high-sampling rates (as fast as 3-minute apart). Moreover, the availability of actual magnitudes of the individual terms in Equation (1) allows to investigate their contribution to the total budget offering further insights in the type of waves occurring during flood wave propagation (Moussa & Bacquillon, 2020; House et al., 2023). This approach is perhaps more powerful in characterizing the wave type than the coarser hysteresis diagnostic approaches such as Mishra & Seth (1996). From this perspective, the availability of additional data on variables and their gradients offered by IVRC and CSA methods might better support the development of new algorithms for hysteresis diagnostic (Lee, 2012). The availability of diagnostic formulas enables to test new or existing monitoring sites for hysteresis presence and severity for each gaging site hence inform on the optimal alternative monitoring the flows.

Given that the implementation and operation of the methods for continuous in-situ streamflow monitoring come with sizable expenses, development of the new measurement approaches have always to be steered by cost-benefit analysis. Transitioning to methods that can continuously and unassisted measure flow velocity (at the surface, along a line, or even at a singular point) and free-surface slopes in addition to discharge using the inverse discharge solution can drastically reduce the operating costs as they do not require development and maintenance of rating curves. The ratings currently used for the popular HQRC stations are cost- and effort-expensive, while the quality of the data is poor for flows slightly deviating from steady conditions and notorious faulty in the area of high flows where the ratings are extrapolated. Along this line, it should be noted that multiple studies show that measuring the free-surface slope or its gradients in Equations (1), (3) and (4) is sufficient to capture well the wave dynamics for the majority of the river sites prone to hysteresis (e.g., Fenton, 2001; Arico et al., 2009; and Dottori et al., 2009). The major problems associated with the free-surface measurements are their accuracy (e.g., Isaak et al., 1999), finding optimal design installations for two measurement locations (where the decision on the appropriate spacing between the station is still open question), and assessing the viability of using slope measurements at one location in conjunction with analytical approximations of light numerical models (e.g., Arico et al., 2009). From this perspective, scrutinizing the capability of the existing and emerging measurement instruments (including ultrasound, lidar, image-based, and remote sensed data) to fulfill more stringent accuracy requirements within reasonable economic feasibility boundaries is a high priority.

## **5. Conclusion**

We have argued here that while the governing relationship used in current monitoring approaches are acceptable for steady and quasi-steady flows, the monitoring methods during unsteady flows should be developed only after these relationships are understood and critical features of the hysteresis behavior are identified to subsequently be used as drivers of the measurement strategies. Such a focus is required when tracking dynamic unsteady water movement in lowland rivers that typically develop severe hysteresis. Such a focus is especially needed in today's nonstationary times when unsteady flows become more prevalent. Such a focus is now possible to undertake with new multivariate monitoring approaches that take advantage of the advancement in the measurement instruments. We hope that the illustrations in this paper made with publicly available in-situ measurements processed with innovative representations are convincing arguments for changing the monitoring paradigms into the future. While the experimental evidence is limited to few illustrations, we attempt to highlight that hysteresis is pervasive and, at times, severe in streams of various characteristics.

Through this paper, we launch a call to action aimed at accelerating the systematic understanding of all hysteresis effects that have immediate consequences on the accuracy of much needed streamflow data for waterway management and scientific investigations. The induced uncertainties produce inconsistent in discharge time series hampering the improvement of the models for streamflow forecasting that to date do not test adequately the movement of the water and transported constituents in space and time. Finally, we argue here that the perhaps the shortest path to fill the knowledge gaps in monitoring unsteady flows is to use the inverse solution of the flow governing equations with explicit use of directly measured variable magnitudes and their spatio-temporal gradients (especially important is the free-surface slope) in the routine practice. Selective implementation of the newly developed monitoring algorithms should necessarily be guided by hysteresis diagnostic criteria and knowledge of the hysteresis sensitivity to hydrological and hydraulic influences.

## **Acknowledgments**

The initial stages of this paper came about during discussions on the Hungarian century-long studies on hysteresis with S. Baranya, R. Csoma, and T. Kramer while the first author was in residence as a Fulbright Scholar Fellow at the Budapest University of Technology and Economics (2022). The authors would like to thank Ryan P. Jackson (USGS Central Midwest Water Science Center) for the supportive and congenial discussions on the hysteresis concept. The first author acknowledges the support provided by the National Science foundation award NSF-EAR-HS 2139649. The second author was supported in this work on the paper by of the NA22NWS4320003 award funded by NWS/NOAA.

## References

- Arcement, G.J., Jr. and Schneider, V.R. (1989). Guide for selecting Manning's roughness coefficients for natural channels and flood plains, U.S. Geological Survey Water-Supply Paper 2339, 38 p.
- Aricò, C., Nasello, C. and Tucciarelli, T. (2009). Using unsteady-state water level data to estimate channel roughness and discharge hydrograph. *Advances in water resources*, 32(8), 1223-1240.
- Bandini, F., Lüthi, B., Peña-Haro, S., Borst, C., Liu, J., Karagkiolidou, S., et al. (2021). A drone-borne method to jointly estimate discharge and Manning's roughness of natural streams. *Water Resources Research*, 57, e2020WR028266. <https://doi.org/10.1029/2020WR028266>
- Baydaroglu, O., Muste, M., Cikmaz, B., Kim, K.D., Demir, I. and Meselhe, E. (2024). Coping with information extraction from in-situ data acquired in natural streams, Submitted to *Hydrological Sciences Journal*, published online at EarthArXiv, <https://doi.org/10.31223/X5S979>
- Cheng, Z., Lee, K., Kim, D., Muste, M., Vidmar, P. and Hulme, J. (2019). Experimental Evidence on the Performance of Rating Curves for Continuous Discharge Estimation in Complex Flow Situations, *J. of Hydrology*, <https://doi.org/10.1016/j.jhydrol.2018.11.021>, pp. 959-971
- Chow, V. T. (1959). *Open channel flow*. London: McGraw-Hill, 11(95), 99,136-140.
- De Sutter, R., Verhoeren, R. and Krein, A. (2001). Simulation of sediment transport during flood events: laboratory work and field experiments, *Hydrological Sciences Journal*, 46:4, 599-610, DOI: 10.1080/02626660109492853
- Dalrymple, T. and Benson, M. A. (1967). Measurement of peak discharge by the slope-area method: U.S. Geological Survey Techniques of Water-Resources Investigations, book 3, chap. A2, p. 12.
- Di Baldassarre, G. and Montanari, A. (2009). Uncertainty in river discharge observations: a quantitative analysis. *Hydrology & Earth System Sciences*, 13(6).
- Dottori, F., Martina, M. and Todini, E. (2009). A dynamic rating curve approach to indirect discharge measurement. *Hydrology and Earth System Sciences*, 13(6), 847-863.
- Feng, D., Fang, K., and Shen, C. (2020). Enhancing streamflow forecast and extracting insights using long-short term memory networks with data integration at continental scales. *Water Resources Research*, 56, e2019WR026793. <https://doi.org/10.1029/2019WR026793>
- Dykstra, S. L. and Dzwonkowski, B. (2020). The propagation of fluvial flood waves through a backwater-estuarine environment. *Water Resources Research*, 56, e2019WR025743, [doi.org/10.1029/2019WR025743](https://doi.org/10.1029/2019WR025743)
- Ewing J. A. (1882). On the production of transient electric currents in iron and steel conductors by twisting them when magnetised or by magnetising them when twisted. *Proc. R. Soc. Lond.* 33, 21–23. [10.1098/rspl.1881.0067](https://doi.org/10.1098/rspl.1881.0067)
- Fenton, J. D. (2001). Rating curves: Part 1 - Correction for surface slope, in *Proc. Conf. on Hydraulics in Civil Engng*, 28-30 Nov., Inst. Engnrs, Aust., Hobart, pp. 309-317.
- Fenton, J. D. (2019). Flood routing methods. *Journal of Hydrology*, 570, 251-264.
- Ferrick, M. G. (1985). Analysis of river wave types. *Water Resources Research* 21, pp. 209–220.
- Gao, P. and Josefson, M. (2012). Event-based suspended sediment dynamics in a central New York watershed. *Geomorphology*, 139-140, 425–437. <https://doi.org/10.1016/j.geomorph.2011.11.007>
- Gellis, A. C. (2013). Factors influencing storm-generated suspended-sediment concentrations and loads in four basins of contrasting land use, humid-tropical Puerto Rico. *Catena*, 104, 39–57. <https://doi.org/10.1016/j.catena.2012.10.018>
- Graf, W. and Qu, Z. (2004). Flood hydrographs in open channels. *Proceedings of the Institution of Civil Engineers-Water Management*, 157(1), 45–52. <https://doi.org/10.1680/wama.2004.157.1.45>
- Harmel, R.D., Cooper, R. J., Slade, R. M., Haney, R. L. and Arnold, J. G. (2006). Cumulative uncertainty in measured streamflow and water quality data for small watersheds, *Transactions of the ASABE* 49(3), pp. 689-701; doi: 10.13031/2013.20488
- Gunawan, B. (2010). A study of flow structures in a two-stage channel using field data, a physical model and numerical modelling, PhD dissertation, University of Birmingham, United Kingdom



- Haddadchi, A. and Hicks, M. (2021). Interpreting event-based suspended sediment concentration and flow hysteresis patterns. *J Soils Sediments* 21, pp. 592–612, <https://doi.org/10.1007/s11368-020-02777-y>
- Hager, W.H., Castro-Orgaz, O. and Hutter, K. (2019). Correspondence between de Saint-Venant and Boussinesq. 1: Birth of the Shallow–Water Equations, *Comptes Rendus Mécanique*, 347(9), pp. 632-662, <https://doi.org/10.1016/j.crme.2019.08.004>.
- Henderson, F.M. (1966). *Open Channel Flow*. Macmillan Series in Civil Engineering; Macmillan Company: New York, NY, USA, p. 522.
- Hirschfeld, S. (1896) A vízrajzi osztály a vízépitészeti kiállításon, *Magyar Mérnök és Építész Egylet közlönye* 30(10), pp. 435—440. (in Hungarian)
- Ho, J., Tull, N., Grzyb, S., Passalacqua, P. and Maidment D. (2022). Understanding factors causing flood wave hysteresis on small streams, *Agua Fall meeting*, December 11-15, San Francisco, CA.
- Hoitink, A.J.F. (2018). Monitoring and analysis of lowland river discharge, *River Flow 2018 - Ninth International Conference on Fluvial Hydraulics*, *E3S Web of Conferences* 40, 06045, [doi.org/10.1051/e3sconf/20184006045](https://doi.org/10.1051/e3sconf/20184006045)
- Holmes, R. (2016). River rating complexity. Constantinescu, editor, *River Flow*, 10-14.
- House, E., Meselhe, E., Muste, M. and Demir, I. (2023). Numerical Modeling of Streamflow Hysteresis to Inform Protocols for Monitoring Unsteady Flow, *AGU Fall meeting*, San Francisco, December 11-15, 2023
- House, E., Meselhe, E., Muste, M. and Demir, I. (2024). Streamflow analysis through a deep dive budget of the Se Venant momentum terms, paper submitted to *Water resources Research* (January, 2024)
- Isaak, D.J., Hubert, W.A. and Krueger, K.L. (199). Accuracy and precision of stream reach water surface slopes estimated in the field and from maps, *North American Journal of Fisheries Management*, 19(1), pp. 141-148, [https://doi.org/10.1577/1548-8675\(1999\)019<0141:AAPOSR>2.0.CO;2](https://doi.org/10.1577/1548-8675(1999)019<0141:AAPOSR>2.0.CO;2)
- Kämäri, M., Tattari, S., Lotsari, E., Koskiahho, J. and Lloyd, C.E.M. (2018). High-frequency monitoring reveals seasonal and event-scale water quality variation in a temporally frozen river, *Journal of Hydrology*, 564, pp 619-639, <https://doi.org/10.1016/j.jhydrol.2018.07.037>.
- Kennedy, E. (1984). Discharge ratings at gaging stations: *US Geological Survey Techniques of Water-Resources Investigations*, book 3, chap. A10, 59.
- Kim, K. (2023). *Hysteresis Diagnostics and Application in River Flow based on Water Surface Slope* (Doctoral dissertation). Dankook University, Yongin, South Korea.
- Knight, D. (2006). *River flood hydraulics: validation issues in one-dimensional flood routing models*: Taylor & Francis, London.
- Kozák, M. (1977). A szabadfelszínü nempermanens vízmozgások számítása digitális számítógép felhasználásával. *Akadémiai Kiadó*, Budapest, Hungary (in Hungarian)
- Kumar, V. (2011). Hysteresis. In: Singh, V.P., Singh, P., Haritashya, U.K. (eds) *Encyclopedia of Snow, Ice and Glaciers*. *Encyclopedia of Earth Sciences Series*. Springer, Dordrecht. [https://doi.org/10.1007/978-90-481-2642-2\\_252](https://doi.org/10.1007/978-90-481-2642-2_252)
- Lee, K. (2013). Evaluation of methodologies for continuous discharge monitoring in unsteady open-channel flows. (Doctoral dissertation). The University of Iowa, Iowa City, Iowa.
- Lee, K., Firoozfar, A.R. and Muste, M. (2017). “Monitoring of Unsteady Open Channel Flows Using Continuous Slope-area Method”, *Hydrol. Earth Syst. Science*, 21 pp.1863-1874; [doi:10.5194/hess-21-1863-2017](https://doi.org/10.5194/hess-21-1863-2017).
- Levesque, V. A. and Oberg, K. A. (2012). Computing discharge using the index velocity method: US Department of the Interior, US Geological Survey.
- Lin, C., Cao, W., Xu, L., Li, D. and Wang, X. (2013). Shear velocity in unsteady channel flows, *Proceedings IAHR World Congress*, ..., Beijing, China.
- Liu, S., Wang, D., Wang, Z., Xu, Z. and Li, D. (2023). Propagation characteristics of the flow and suspended sediment peaks in the three gorges reservoir, China: Insight from numerical simulations and measured data. *Hydrological Processes*, 37(10), e15000. <https://doi.org/10.1002/hyp.15000>

- Lloyd, C. E. M., Freer, J. E., Johnes, P. J. and Collins, A. L. (2016). Testing an improved index for analysing storm discharge–concentration hysteresis, *Hydrol. Earth Syst. Sci.*, 20, pp. 625–632, <https://doi.org/10.5194/hess-20-625-2016>, 2016.
- Mallakpour, I., Villarini, G. (2015). The changing nature of flooding across the central United States. *Nature Clim Change* 5, pp., 250–254, <https://doi.org/10.1038/nclimate2516>
- Marcus, N. G., Rápalo, L.M.C, Oliveira, P.T.S., Giacomoni, G.H., do Lago, C.A.F. and Mendiondo, E.M. (2023). Modeling unsteady and steady 1D hydrodynamics under different hydraulic conceptualizations: Model/Software development and case studies, *Environmental Modelling & Software*, 167, <https://doi.org/10.1016/j.envsoft.2023.105733>.
- McDonnell, J. J. and K. Beven (2014). Debates—The future of hydrological sciences: A (common) path forward? A call to action aimed at understanding velocities, celerities, and residence time distributions of the headwater hydrograph, *Water Resources Research*, 50, pp. 5342–5350, doi:10.1002/2013WR015141.
- Mishra, S. K. and Seth, S. M. (1996). “Use of hysteresis for defining the nature of flood wave propagation in natural channels.” *Hydrological Sci.*, 41(2), 153–170.
- Mishra, S. K. and Vijay P. S. (2001). Hysteresis-based flood-wave analysis using the concept of strain, *Hydrological processes*, 15(9), pp 1635-1651, doi:10.1002/hyp.225.
- Moots, E. (1938). A study in flood waves—University of Iowa Studies in Engineering. Bull, 14. <https://ir.uiowa.edu/cgi/viewcontent.cgi?article=1014&context=uisie>
- Moussa, R. and Bocquillon, C. (2000). Approximation zones of the Saint-Venant equations flood routing with overbank flow, *Hydrol. Earth Syst. Sci.*, 4, pp. 251–260, <https://doi.org/10.5194/hess-4-251-2000>
- Mrokowska, M., Rowinski, P. and Kalinowska, M. (2015). A methodological approach of estimating resistance to flow under unsteady flow conditions. *Hydrology & Earth System Sciences*, 19(10), 4041–4053. <https://doi.org/10.5194/hess-19-4041-2015>
- Mrokowska, M.M., Rowiński, P.M., Książek, L., Strużyński, L., Wyrębek, M. and Radecki-Pawlik, A. (2018). Laboratory studies on bedload transport under unsteady flow conditions, *Journal of Hydrology and Hydromechanics*, 66, pp. 23-31, DOI: 10.1515/johh-2017-0032
- Muste, M., Bacotiu, C. and Thomas, D. (2019). Evaluation of the slope-area method for continuous streamflow monitoring, *Proceedings of the 38th World Congress, Panama City, Panama*
- Muste, M., Lee, K., Kim, D., Bacotiu, C., Rojas Oliveros, M., Cheng, Z. and Quintero, F. (2020). “Revisiting Hysteresis of Flow Variables in Monitoring Unsteady Streamflows” *State-of-the-art Paper Series, Journal of Hydraulic Research*; 58(6), pp. 867-887, <https://doi.org/10.1080/00221686.2020.1786742>
- Muste, M., Kim, D. and Kim, K. (2022a). Insights into flood wave propagation in natural streams as captured with acoustic profilers at an index-velocity gaging station, 14(9), *Water, Special Issue Lowering Risk by Increasing Resilience: Selected Papers from 8th International Conference on Flood Management (ICFM 8)*, <https://doi.org/10.3390/w14091380>.
- Muste, M., Kim, D. and Kim, K. (2022b). A flood-crest forecast prototype for river floods using only in-stream measurements, *Communications Earth & Environment*, <https://doi.org/10.1038/s43247-022-00402-z>
- Nezu, I. and Nakagawa, H. (1995). Turbulence measurements in unsteady free-surface flows. *Flow measurement and Instrumentation*, 6(1), 49-59.
- Paul, J. D., Buytaert, W. and Sah, N. (2020). A technical evaluation of lidar-based measurement of river water levels. *Water Resources Research*, 56, e2019WR026810, <https://doi.org/10.1029/2019WR026810>
- Perret, E., Lang, M. and Le Coz, J. (2022). A framework for detecting stage-discharge hysteresis due to flow unsteadiness: Application to France’s national hydrometry network, *Journal of Hydrology*, 608, <https://doi.org/10.1016/j.jhydrol.2022.127567>.
- Prowse, C. W. (1984). Some thoughts on lag and hysteresis. *Area*, 16(1), 17–23.

- Rantz, S. E. (1982). Measurement and computation of streamflow (Vol. 2175). US Department of the Interior, Geological Survey
- Rátky, I. (2000) Árvízi hurokgörbék közelítő számítása. *Vízügyi Közlemények* 82(2), pp. 232—261(in Hungarian)
- Rowinski, P. M., Czernuszenko, W. and Pretre, J.-M. (2000). Time-dependent shear velocities in channel routing. *Hydrological Sciences Journal*, 45(6), 881–895.  
<https://doi.org/10.1080/02626660009492390>
- Saint-Venant, Barre de (1871). Theory of unsteady water flow, with application to river floods and to propagation of tides in river channels, *Acad. sci. Comptes rendus*, v. 73, p. 148-154, 237-240. (Translated into English by U.S. Corps of Engineers, no. 49-g, Waterways Experiment Station, Vicksburg, Miss., 1949.).
- Schmidt, A.R. (2002). Analysis of Stage-discharge Relations for Open Channel Flows and their Associated Uncertainties. Ph.D. Thesis, University of Illinois at Urbana-Champaign, IL, USA.
- Schmidt, A. R. and Garcia, M. H. (2003). Theoretical Examination of Historical Shifts and Adjustments to Stage-Discharge Rating Curves. In P. Bizier, & P. DeBarry (Eds.), *World Water and Environmental Resources Congress* (pp. 1089-1098). (World Water and Environmental Resources Congress), DOI:10.1061/40685(2003)233
- Smith, C. F., Cordova, J. T. and Wiele, S. M. (2010). The continuous slope-area method for computing event hydrographs (2328-0328). Retrieved from U. S. Geological Survey
- Tabarestani, M. K. and Zarrati, A. (2015). Sediment transport during flood event: A review. *Int. Journal Environmental Science & Technology*, 12(2), 775–788, doi.org/10.1007/s13762-014-0689-6
- Thébault, C., Perrin, C., Andréassian, V., Thirel, G., Legrand, S. and Delaigue, O. (2023) Impact of suspicious streamflow data on the efficiency and parameter estimates of rainfall–runoff models, *Hydrological Sciences Journal*, 68:12, 1627-1647, DOI:10.1080/02626667.2023.2234893
- Wunsch C (2019). Inverse Problems, Inverse Methods, and Inverse Models. In Cochran, J. Kirk; Bokuniewicz, J. Henry; Yager, L. Patricia (Eds.) *Encyclopedia of Ocean Sciences*, 3rd Edition. vol. 5, pp. 502-512, Elsevier, dx.doi.org/10.1016/B978-0-12-409548-9.11262-X
- Zuecco, G., Penna, D., Borga, M. and van Meerveld H. J. (2015). A versatile index to characterize hysteresis between hydrological variables at the runoff event timescale, *Hydrological processes*, 30(9), pp. 1449-1466, <https://doi.org/10.1002/hyp.10681>
- Yevjevich, V. M. (1964). Bibliography and discussion of flood-routing methods and unsteady flow in channels, U.S. Geological Survey Water-supply paper 1690, U.S. Government Printing Office, Washington, D.C.
- Yoshida, K, Kajikawa, Y., Nishiyama, S., Islam, M.D. T., Adachi, S and Sakai, K. (2023) Three-dimensional numerical modelling of floods in river corridor with complex vegetation quantified using airborne LiDAR imagery, *Journal of Hydraulic Research*, 61:1, 88-108, DOI: 10.1080/00221686.2022.2106596